MECHANICAL, DIFFUSION AND DEGRADATION PROPERTIES OF BLENDS OF CELLULOSE AND RECYCLED LOW DENSITY POLYETHYLENE

OTIENO GEORGE WERE (B.ED. Sc)
I56/CE/10382/2007

A thesis submitted in partial fulfillment of the requirements for the award of the degree of Master of Science in the School of Pure and Applied Sciences of Kenyatta University

30th May, 2013

DECLARATION

I declare that the work presented in this thesis is my original work and has never been presented for the award of any degree in any university

Otieno George Were

Signature……..Date…….

Department of Physics

Kenyatta University

We confirm that the candidate carried out the work reported in this thesis under our supervision

Supervisors

Dr. Merenga A. S.

Signature……Date……..

Department of Physics

Kenyatta University

Dr. Migwi C. M.

Signature ……Date……..

Department of Physics

Kenyatta University

DEDICATION

This thesis is dedicated to my friend and wife Lindah and dear sons Hope and Rieko

ACKNOWLEDGEMENTS

Foremost, I would like to sincerely thank my thesis advisors; Dr. Abdallah S. Merenga and Dr. Charles M. Migwi for their able guidance and support during my research period and helping me attain the research objectives. A lot of thanks go to the chairman Physics department, Kenyatta University Dr. Njoroge for being supportive throughout this work. Similar thanks to Dr. Singh, the chairman D.B.P.S, Physics department for his guidance during the thesis writing. This project involved a lot of laboratory work. I am very grateful to all the Physics department technical staff led by Mr. Simon Njuguna who made the Laboratory accessible for me, and generally did things that were beyond the call of duty. I was blessed to be surrounded by supportive colleagues: Agan, Korir, Muga, Mbithi, Ketui, Kundu, Tuwei, and Munguti. Special thanks go to the Principal Maseno School for unwavering support during my studies. May God richly bless you. To my parents: Thank you for your unconditional love and support. In your demise, dad, you are my inspiration and the embodiment of integrity, courage, and honor. Mom, thanks for your undying kindness and care. You are the anchor that has kept our family going in the absence of our dad. Finally, the most important part of my life is my family. I would never have been able to accomplish any of my goals without the support of my wife, Lindah Ojwang' and my sons, Hope and Rieko. I love you with all of my heart. I will never be able to express all of my gratitude. You had faith in me and what I was doing even when I had lost it. Thank you for all of your help and sacrifice. I hope someday I could provide as much help and support for my children. I love you and thank you. Above all I want to thank the Almighty God who has taken me this far. I confess that the strides I have made were only possible because He was my strength and motivator.

TABLE OF CONTENTS

LIST OF TABLES

LIST OF FIGURES

LIST OF SCHEMES

ABBREVIATIONS, SYMBOLS AND ACRONYMS

β	Heating rate
C	Carbon
C	Concentration
CEL	Cellulose
CoA	Coenzyme A
CQ	Camphorquinone
D	Diffusion coefficient
Δ	Delta
DMA	Dynamic Mechanical Analysis
ε	Strain
ε^*	Complex Strain
E_a	Activation energy
E_1 and E_2	Spring constants
E^*	Complex modulus
$E(\omega)$	Tensile Modulus
$E'(\omega)$	Storage modulus
$E''(\omega)$	Loss modulus
ENR50	Epoxidised natural rubber
f	Frequency
FAD	Flavin Adenine Dinucleotide enzyme
h	Thickness
HDPE	High density polyethylene

IMD	In-mould decoration
J	Diffusive flux
J_t	Creep compliance
k	Boltzmann constant
LDPE	Low density polyethylene
LLDPE	Linear low density polyethylene
M	Amount of diffusant
MCS	Methylated-cornstarch
N	Order of reaction
NAD	Nicotinamide adenine dinucleotide enzyme
R	Recovery
R: C	RLDPE: CEL
RLDPE	Recycled low density polyethylene
SLS	Standard linear solid
t	Time
T	Absolute temperature
T_g	Glass transition temperature
τ	Relaxation time
τ_0	Preexponential factor
TCA	Tricarboxylic acid
TGA	Thermogravimetric analysis
V	Total volume
V^*	Minimum volume

V_m	Mean volume
V_o	volume
VFT	Vogel−Fulcher-Tamman
WLF	William-Landel-Ferry
x	Position
α	Volume thermal expansion coefficient
η	Viscosity
σ	Stress
σ^*	Complex Stress
α	Volume thermal expansion co-efficient
ω	Angular frequency
y	weight response

ABSTRACT

Recycled Low Density Polyethylene waste pollutes the environment since it is non-biodegradable. This work investigates the enhancement of disposal of these wastes without compromising their tensile strength and permeability by blending Recycled Low Density Polyethylene with Cellulose. Injection molded blends of Recycled Low Density Polyethylene and Cellulose were prepared in percentage ratios of 100:0, 95:5, 90:10, 85:15 and 80:20. Dynamic mechanical analysis, creep, diffusion, thermal degradation and biodegradation measurements were carried out on the molded samples. The dynamic mechanical analysis was carried out in the frequency range from 1 to 30 Hz and at a temperature range from -30 °C to 90 °C. Three relaxation processes namely; α, β_1 and β_2 were observed. The α process is assigned to large scale chain motion where as β_1 and β_2 suggest lamellae shear of two different thicknesses. The intensities of the processes decreased with increase in cellulose loading whereas the temperature shifts were not observed. Creep testing and creep recovery testing were carried out at 30 °C, 40 °C, 50 °C and 60 °C by applying a constant stress. Creep strain increased moderately with increasing loading intakes. Incorporation of cellulose decreased recovery. The time- temperature superposition principle was applied to predict the long term (10^8 s) creep behavior. Deformation behavior follows WLF law suggesting that free volume plays a crucial role. The influence of water environment on the sorption characteristics of RLDPE-CEL blend was studied by immersion in water at room temperature. The effects of cellulose loading on the sorption behavior were also evaluated. Water uptake was found to increase with cellulose loading. Weight change profiles for the blends at room temperature indicated that the diffusion is Fickian. Diffusion coefficients increased with cellulose intake. Thermo-gravimetric analysis (TGA) was carried out on the blends using Lindberg Blue tube furnace (TF 55035C-1) from 80 to 620 ^{o}C at a heating rate of 5 ^{o}C/ minute. The decomposition trend shifted from one stage to two stage with increasing cellulose intake. Biodegradation was determined by burial technique. After designated times, the degraded sheets were taken out of soil, rinsed carefully with water, and then dried at 50 ºC until the consecutive weights obtained were the same. The models of analysis for DMA and Creep data were VFT and WLF respectively. Thermal degradation data was analyzed using Arrhenius laws while Fick's laws were used in diffusion measurements. Biodegradation was enhanced with cellulose intake thus the composites can be adopted by policy makers to minimize environmental pollution.

CHAPTER ONE

INTRODUCTION

1.1 Background to the Study

The world rate of production of plastics is approximately 100 million tonnes per annum (Hannequart, 2004). This will eventually be disposed and will result in a significant proportion in municipal solid waste. Attempts have been made to recycle the post-consumer plastics in order to reduce the environmental impact and consumption of virgin plastics. Recycled Low Density Polyethylene (RLDPE) is a form of polyethylene having many side branches off the main carbon backbone and a less closely packed structure than that of High Density Polyethylene (Speight and Norbert, 2005). Recycled Low Density Polyethylene has weaker intermolecular forces (instantaneous-dipole induced-dipole attraction), its strength is lower, and its resilience is higher (Madsen and Lilholt, 2003). Despite the generally excellent properties of Recycled Low Density Polyethylene, there is still need to modify and regulate its properties through blending with cellulose which is a biodegradable polymer (Bodor, 1991). As a result, the use of natural/bio-fiber reinforced composites has been rapidly expanded due to the availability of natural/bio-fibers derived from annually renewable resources, for use as reinforcing fibers in both thermoplastic and thermosetting matrix composites as well as for the positive environmental benefits gained by such materials (Huda *et al.*, 2005). Knowing the long-term behavior of these polymers is also essential to estimate their life-time under load.

There has been tremendous increase in the use of RLDPE, particularly in agriculture and domestic sectors (Kahovec *et al.*, 2002). This has resulted into increased production and

associated disposal problem. RLDPE in its pure form is extremely resistant to environmental degradation. An alternative approach that can be used to keep the environment free of wastes would be to use an incinerator. Incineration would always produce a large amount of carbon dioxide and other toxic gases which eventually contribute to global pollution.

Based on these backgrounds, there is an urgent need for the development of ‘‘green polymeric materials’’ that does not involve the use of toxic or noxious components in their manufacture and that can degrade into natural environmental products faster. The addition of biodegradable components facilitates the destruction of RLDPE materials under the influence of microorganisms and environmental actions (Huang, 1984). Cellulose is one of the strongest and stiffest fibers available and it has a high potential to act as reinforcing agent in biopolymers. Mechanical properties of cellulose-plastic composites, such as stiffness, strength, impact resistance etc., play an important role in determining the suitability of these products in various applications. Cellulose-based polymer composites are characterized by low cost, desirable fiber aspect ratio, low density, high specific stiffness, high tensile strength, biodegradability and flexibility during processing with no harm to the equipment, and good mechanical properties (Huda *et al.,* 2005). Among natural polymers a special attention should be drawn to a renewable and almost inexhaustible source of raw materials – cellulose. The synthetic polymers such as industrial polyolefins show high mechanical and thermal characteristics; they are stable against the action of microorganisms and are incapable of biodegradation, whereas the natural polymers characterized by biodegradability exhibit good mechanical properties (Arvanitojannis, 1999).

The materials, obtained from these polymer blends can be used as permeable membranes, films for food products, and articles for short-term use since they are environmentally friendly, unlike synthetic polymers. In this way the investigation of thermal stability and combustibility of these materials is very important. RLDPE-CEL blends therefore offer a new class of materials which can minimize pollution.

Permeation of solvent through a polymeric membrane is commonly used in several industrial processes. Consequently the transport properties, (i.e. the diffusion coefficients) within a certain polymer matrix and the evaporation/desorption from film surface, play an important role in preserving the antioxidant efficiency. This can be used for the long-term applications in polymer materials such as RLDPE (Scoponi *et al.*, 2000). In particular, stabilizer persistence is a fundamental requirement for food packaging applications, where the food contamination due to the stabilizer diffusion should be avoided for human health concerns. It is believed that this study will give an insight into the diffusion processes of some conventional additives used as thermal stabilizers in new commercially available RLDPE packaging materials. There is need to investigate diffusivity in RLDPE-CEL blends. These results will be useful for perfecting our membrane design method. The rate at which water is absorbed by a composite depends on many variables including fiber type, matrix, temperature, the difference in water distribution within the composite, reaction between water and the matrix, among others (Wright and Mathias, 1993). Both the rate of water pick-up and the total amount of moisture absorbed depend on the chemical structure of the resin and crosslinking agent together with the temperature and relative humidity (George *et al*., 1998). Moisture diffuses into a polymer to vary-

ing degrees depending upon molecular and micro structural aspects such as polarity, the extent of crystallinity of thermoplastics and the presence of residual hardeners or other water-attracting species (Joseph *et al.,* 1998). The purpose of blending polymers is to gain synergistic improvement in properties at both micro and macro levels. Thermal stability, strength, diffusivity and biodegradability are among the properties that can be improved by these blends. The low cost and high specific properties of CEL imply a significant property potential for the commodity synthetic polymers (Harikumar *et al.,* 1999). Biodegradable plastics offer a lot of advantages such as, low accumulation of bulky plastic materials in the environment and reduction in the cost of waste management (Coutinho *et al.,* 2000).

Several studies on the molecular dynamics of RLDPE have been reported (Cowle *et al.,* 1991). However, identifying the molecular origin of these secondary relaxations has proven to be a difficult task. In this respect the presence of the hydroxyl groups in CEL creates an environment which influences the relaxation processes (Peng *et al.,* 2002). DMA, creep, diffusion, thermal degradation and biodegradability of the RLDPE are methods of monitoring property changes in models and damping as a function of stress, temperature, frequency and sorption or a combination of these quantities and they were used in this work (McCrum *et al.,* 2003). DMA monitored relaxation processes, creep monitored strain at constant stress, dipping the samples in pure water revealed diffusivity while TGA and soil burial test revealed thermal degradation and biodegradability respectively.

1.2 Statement of the Research Problem

Disposal of plastic wastes have been a major challenge since most plastics do not easily degrade. This has compelled the handlers to burn them after use. Burning plastics poses an environmental threat as they emit harmful fumes. This work investigates the enhancement of disposal of these wastes without compromising their tensile strength and permeability by blending Recycled Low Density Polyethylene with Cellulose. The effect of CEL concentration in RLDPE-CEL blends on mechanical, diffusion and degradation properties was investigated. Cellulose being a biodegradable polymer was expected to enhance the degradation of disposed Recycled Low Density Polyethylene wastes, reduce the toxicity during burning and improve packaging characteristics through effective permeability. A combination of DMA, creep, diffusion, thermal degradation and biodegradability measurements were used to study their relationship with varying CEL concentrations.

1.3 Objectives of the Research Study

1.3.1 Main Objective

To carry out measurements on mechanical, diffusion and degradation properties in RLDPE-CEL blend.

1.3.2 Specific Objectives

To investigate the effect of cellulose concentration in RLDPE-CEL blends on:

(i) Storage and loss modulus as a function of temperature and frequency

(ii) Creep modulus and recovery as a function of temperature

(iii) Diffusion behavior as a function of time

(iv) Thermal degradation as a function of time

(v) Biodegradability as a function of time

1.4 Rationale of the Research Study

Time dependent properties of RLDPE can be enhanced through blending it with CEL. Stiffness and long term creep performance of RLDPE is of particular importance as it finds increased use in structural building products. In order to optimize polymer selection and design for specific application, it is important to investigate the origin of physical properties in molecular structure and to control the structure by processing. The injection molding process has been found to influence the molecular dynamics in RLDPE. Chain motions are closely linked to the mechanical properties of the polymer. The inter-chain interactions affect the molecular dynamics in polymers. Also, their degradation is imperative because RLDPE wastes cause litter problem. Their use as packaging materials is also unsatisfactory. It was of interest to investigate the effect of CEL on the molecular dynamics of injection molded samples. A comparison was made on the effect of CEL on RLDPE.

RLDPE applications always involve stress due to load bearing. Dynamic mechanical tests provide information about viscoelastic properties and molecular relaxations. Any mechanical property may be influenced by temperature and hence the need to perform the tests at various temperatures.

CHAPTER TWO

LITERATURE REVIEW

2.1 Recycled polymers

Polymers are synthesized for various applications (Sax, 2010). However, their properties must satisfy particular application needs which can be met through blending. Goran *et al* (2010) studied silane-crosslinking of recycled low-density polyethylene wood composites and its effect on composites properties. The flexural strength was doubled compared to uncrosslinked samples and the creep strain was reduced. Alamri *et al* (2012) found that Epoxy nanocomposites reinforced with recycled cellulose fibres significantly enhanced flexural strength, fracture toughness, impact strength and impact toughness of the composites. However, the presence of either nanoclay or recycled cellulose fibres accelerated the thermal degradation of neat epoxy. At high temperatures, thermal stability was enhanced with increased char residue over neat resin. The introduction of recycled glass fibers in hybrid composites provided an improved water absorption behavior compared to that of Wood plastic composites with equal amounts of filler (Marco *et al.*, 2011).

According to González *et al* (2011), the recycled HDPE-matrix composites showed a ‘‘fall’’ in the shear viscosity curves at low shear rates, ultimately due to the thermal degradation of the cellulose fibers of the composites during the first stages of the rheological testing. Bernasconi *et al* (2007) did analysis of the effect of mechanical recycling upon tensile strength of a short glass fibre reinforced polyamide 6,6 and the tensile test results showed a decrease of both elastic modulus and tensile.

Alcock *et al* (2008) investigated the effect of temperature and strain rate on the impact performance of recyclable all-polypropylene composites and found that unlike isotropic Polypropylene, the highly oriented nature of all- Polypropylene composites means that a significant influence of glass transition temperature is not observed and so all- Polypropylene composites retain high impact energy absorption even at low temperatures.

2.2 Other polymer blends

According to Krishnan and Rex (2012), addition of Harakeke (Phormium tenax) fibre to waste plastics showed improvement of tensile and impact properties due to reduction of the tendency of waste plastic to exhibit localised thinning. Alhuthali *et al* (2012) added recycled cellulose fibre to vinyl-ester nanocomposites and found that there was improved fibre-matrix addition giving greater strength property results.

Addition of natural flax fibre to HDPE showed significant enhancement of toughness (Singletone *et al.,* 2003). Addition of cellulose pulp fibres improved mechanical, rheological and thermal properties (Anamaria *et al.,* 2012). Addition of chromated copper arsenate- treated wood flour to RHDPE led to higher modulus of elasticity and rupture (Kamdem *et al.,* 2004).

Thermal, rheological and mechanical characterizations were carried out on neat HDPE and HDPE/reed fibre (Phragmite australis) composites by Kraiem *et al* (2012) and the results showed that reed fibre may be an accelerating factor for the degradation of the polymer, while confirming the stability of composites.

Mehdi *et al* (2003) investigated creep strain versus time at five different temperatures for Kenaf-Fiber/High-Density Polyethylene Composite and found that the log of strain increased with the log of time and also with temperature. According to Yanjun *et al* (2011) while studying creep analysis of bamboo high-density polyethylene composites, the time temperature superposition technique produced smooth master creep curves through horizontal shifts, but it slightly over-predicted the long-term creep for most composite systems.

Chandra and Renu (1997) studied LLDPE/starch blends and found that in all the compositions, water absorption and opacity increased with increasing amount of starch in the blends. Me´tayer *et al* (1999) tested various polymers with respect to water and found that LDPE showed significant hydrophobic properties. Suda *et al* (2001) observed that the water absorption of the modified starch-filled LDPE sheets was higher than that of the unmodified ones. Ioannis *et al* (1998) extruded blends of LDPE and rice or potato starch in the presence of varying amounts of water, hot pressed and studied it with regard to their mechanical properties and their gas/water permeability and biodegradability before and after storage. The presence of high starch contents (30 %, w/w) had an adverse effect on the mechanical properties of LDPE-starch blends. Eleni *et al* (1998) found out that gas permeability and water vapour transmission rate increased proportionally with the starch content in the LDPE-starch blend.

Hirata (1974) reported two processes occurring during the thermal decomposition of CEL: an initial reaction and a propagation reaction. Mamleev *et al* (2009) proposed a two step kinetic model to explain all observable phenomena related to the pyrolysis of CEL,

describing mass loss by two competing pathways of CEL degradation, transglycosydation and elimination. Herrera *et al* (2005) did thermogravimetric analysis in a nitrogen atmosphere and found that the addition of CEL (0-50 wt%) lowered the thermal resistance of LDPE-CEL biocomposites. The onset degradation temperature and the decomposition temperature of the composites of LDPE and CEL are increased when CEL is added to LDPE in a nitrogen atmosphere (Behjat, 2009). Prut and and Zelenetskii (2001) found that the thermal degradation of cellulose and ethylcellulose as additives to LDPE blends show a decrease of apparent activation energies as compared with pristine cellulose and ethylcellulose.

LDPE cannot be easily degraded by microorganisms since it is a stable polymer, and consists of long chains of ethylene monomers. However, it was reported by Tsuchii *et al.* (1980) that lower molecular weight LDPE oligomers were partially degraded by *Acinetobacter* sp. 351 upon dispersion, while high molecular weight LDPE could not be degraded. Blending of LDPE with additives generally enhances auto-oxidation, reduces the molecular weight of the polymer and then makes it easier for microorganisms to degrade the low molecular weight materials. It is worthy to note that despite all these attempts to enhance the biodegradation of LDPE blends, the biodegradability with microorganisms on the LDPE part of the blends is still very low (Hakkarainen *et al.*, 2004). Biodegradability of low density LDPE-starch blends was enhanced with compatibilizer (Bikiaris *et al.,* 1998). Percentage crystallinity decreased as the starch content increased and biodegradation resulted in an increase of crystallinity in LLDPE-starch blends (Chandra *et al.*, 1997).

According to Khalid *et al* (2009), the *E'* of oil palm empty fruit bunch- filled PP biocomposites was found to be higher than that of pure PP, because incorporation of biofiller increased the stiffness of the biocomposites. They also reported a decline in *E''* at higher temperatures and associated it with the increasing viscosity and chain mobility of the polymer matrix.

The constituent polymers and their ratios in the blend govern the glass transition temperature and the extent of the associated fall in storage modulus (Crawford, 1981). Groeninckx *et al* (1979) found that the time superposition principle was not applicable in the temperature range between the glass transitions of two polymers forming a blend and the shift factors are a function of time in addition to temperature. Aroni *et al* (2001) measured creep in uniaxial extension in starch/synthetic polymer blends and found the compliance of these blends to have increased with increasing applied stress and temperature and decreased with increasing starch content. They calculated WLF constants based on the empirical shift factors and they were in the range obtained for other polymers.

The highly hydrophilic nature of natural fibers results from their hydroxyl groups (Lee, 2005). Yew *et al* (2005) reported that the kinetics of water absorption of the PLA-RS composites conforms to Flick's law and the *D* value in PLA-RS composite are higher than that of neat PLA. According to Russell *et al* (2001), while the 'slow theory' predicts that the tracer diffusion coefficient *D* is controlled by the diffusion of the slower-moving component, 'fast theory' says it is controlled by the diffusion of the faster-moving one. Jiulin and Wang (1999) studied probe diffusion of camphorquinone (CQ) in a polystyrene (PS)-poly (2, 6-dimethyl-1, 4-phenylene oxide) (PPO) blend using the laser-induced ho-

lographic grating relaxation technique. At a fixed temperature above T_g, they found that the logarithm of the probe diffusion coefficient varies linearly with the weight fraction of PS or PPO. Zhao *et al* (2006) reported that better water resistance could be obtained for the cornstarch/PVA film on methylation of cornstarch, while higher water resistance of the MCS/PVA film could not be expected by increasing the degree of substitution of the modified starch. Ramazan *et al* (2007) in his study on moisture absorption behavior of palm/PP composite reported that the amount of moisture absorbed at saturation by PP during immersion in water increased significantly by introduction of palm fiber in the polymer.

According to Levchik and Weil (2006) different blends of polyethylene terephthalate with different impact modifiers showed a minimum of thermal activation energy, which indicates an interaction between decomposition products. According to Khalid *et al* (2009), thermogravimetric analysis of oil palm empty fruit bunch- filled PP biocomposites showed a decrease in thermal stability and degradation temperature and increase in ash content.

Despite the researches that have been done on RLDPE and cellulose, none has dealt with the mechanical, degradation and diffusion analysis of RLDPE-CEL blend. This research is intended to give an insight into the recovery and sorption properties of blends of RLDPE with CEL.

CHAPTER THREE

THEORETICAL CONSIDERATIONS

3.1 Dynamic Mechanical Analysis

Dynamic mechanical analyzer (DMA) yields information about the mechanical properties of a specimen placed in minor, usually sinusoidal, oscillation as a function of time and temperature by subjecting it to a small, usually sinusoidal, oscillating force. For static measurements, the parameters used to specify the mechanical properties of an isotropic medium in the absence of relaxation effects are stress (σ) and strain (ε). The applied mechanical load, that is, stress, elicits a corresponding strain (deformation) given by the relationship shown in equation 3.1.

$$\sigma = E\,\varepsilon \qquad (3.1)$$

where E is the tensile modulus. The modulus is often known as the rigidity and is a quantity that is a representative of the materials resistance to deformation. Its reciprocal is the compliance, J (McCrum *et al.*, 2003).

If a material is purely viscous, the phase difference is 90^{o}. However, most materials including polymers are viscoelastic and both behave as elastic (Hookean) solid and viscous (Newtonian) liquid, such materials exhibit a phase difference between the extremes. This phase difference, together with the amplitudes of the stress and strain waves, is used to determine a variety of fundamental material parameters, including storage and loss modulus, loss factor (tan δ), complex and dynamic viscosity, storage and loss compliance, transition temperatures, creep, and stress relaxation as well as related performance

attributes such as rate of degree of cure, sound absorption, impact resistance and morphology (McCrum *et al.*, 2003).

Dynamic mechanical analysis measures the viscoelastic properties using either transient or dynamic oscillatory tests. Transient tests include creep and stress relaxation. In a creep relaxation, a stress is applied on a sample and held constant while the deformation is measured versus time. After a short time, the stress is removed and the recovery is measured as a function of time. In a stress relaxation, a deformation is applied to the sample and held constant, and the degradation of the stress required in maintaining the deformation is measured as a function of time. The sample is then released to an unstressed state, and its recovery is measured as a function of time. The dynamic oscillatory test is the most common, where a sinusoidal stress (or strain) is applied to a material and the resultant sinusoidal strain (or stress) is measured. Most DMA measurements are made using a single frequency and constant deformation (strain) amplitude while varying temperature (McCrum *et al.*, 2003).

3.1.1 Dynamic mechanical measurement (complex modulus)

An alternative experimental procedure to creep and stress relaxation is to subject the specimen to an alternating strain and simultaneously measure the stress (Ward and Hadley, 1993). For linear viscoelastic behavior, when the equilibrium is reached, the stress and strain vary sinusoidally, but the strain lags behind the stress. If stress $\sigma(t)$ is applied, then altered with time t and angular frequency ω the governing equation is

$$\sigma(t) = \sigma_o \sin \omega t \qquad (3.2)$$

where σ_o is the amplitude. An ideal elastic body's deformation instantly follows an applied stress, and consequently,

$$\varepsilon(t) = \varepsilon_o \sin \omega t \qquad (3.3)$$

Polymers are viscoelastic materials thus deformation (strain) lags behind the applied stress as shown in Figure 3.1.

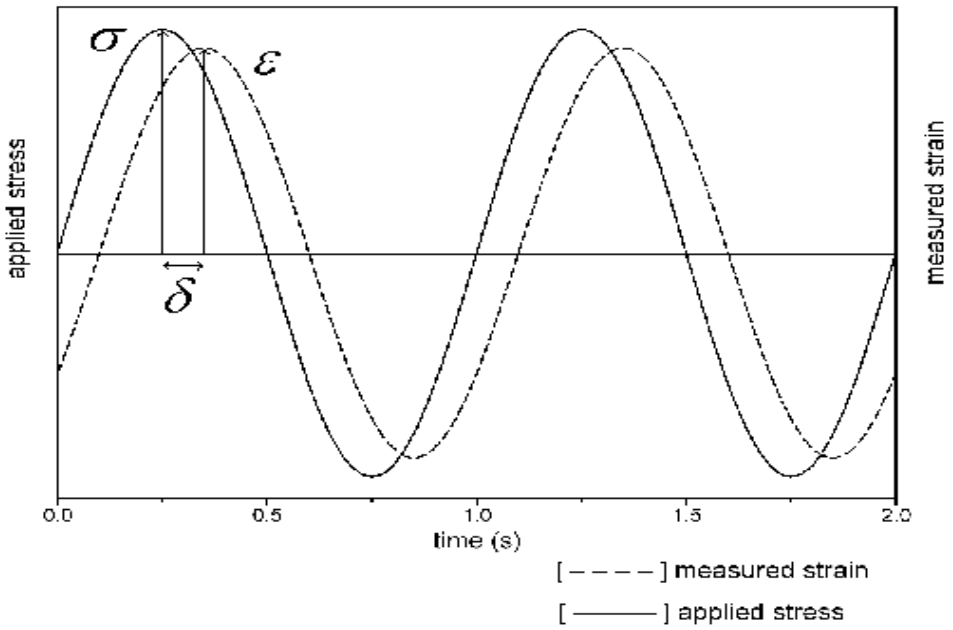

Figure 3.1: Stress and strain as a function of time with dynamic (sinusoidal) loading (Strain) (Ward and Hadley, 1993)

In ideal viscoelastic materials, the resulting phase angle δ in the corresponding vector diagram can be assumed to be constant, such that the deformation follows equation 3.3 while the stress is given by equation 3.4

$$\sigma(t) = \sigma_o \sin(\omega t + \delta) \qquad (3.4)$$

The stress vector can be considered to be the sum of two components. One component, σ' = σo cos δ, is in phase with the deformation, the other component, on the other hand, σ" = σo sin δ, is out of phase. A modulus can be assigned to each of the components. The real modulus, or storage modulus, *E*', measures the rigidity and resistance to deformation of the sample. It is related to the complex modulus of rigidity E* by equation 3.5

$$E' = \sigma' / \varepsilon_o = (\sigma_o / \varepsilon_o) \cos \delta = E^* \cos \delta \qquad (3.5)$$

The imaginary or loss modulus, *E"*, given as equation 3.6, reflects the loss of useful mechanical energy through dissipation as heat.

$$E'' = \sigma'' / \varepsilon_o = E^* \sin \delta \qquad (3.6)$$

The loss factor spectra *E"* can be quantitatively described by a superposition of model function and given in equation 3.7 (Vauderschueren *et al.*, 1979).

$$E''(T) = \sum_{i=1}^{2} A_i \exp\left\{ -\frac{E_i}{kT} - \frac{T^2}{T_{m_i}^2} \exp\left[\frac{E_i}{k}\left(\frac{1}{T_{m_i}} - \frac{1}{T} \right) \right] \right\} \qquad (3.7)$$

In this model function, A is a constant, k Boltzmann constant, T absolute temperature, T_m temperature representing maximum loss modulus, E_i is the activation energy and i refers to different processes which contribute to the mechanical response.

The loss factor, storage modulus and loss modulus vary with frequency of loading as shown in Figure 3.2. At low frequency the polymer is rubber like and has a low storage modulus, which is independent of frequency. At high frequency, the polymer is glassy and the storage modulus is again independent of frequency. In the intermediate region where the material behaves viscoelastically, the storage modulus increases with increasing frequency. As the frequency is increased it becomes more difficult for the chains to

respond to the applied forces and tend to remain in a frozen state. A frozen system stores more energy than a free system (Ward and Hadley, 1993).

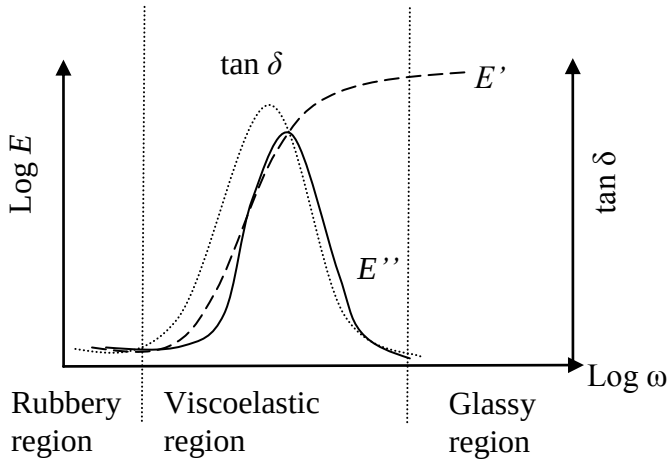

Figure 3.2: The complex modulus, E*=E'+iE", as a function of frequency (Ward and Hadley, 1993)

The phase angle, expressed as its sine or tangent, is an important parameter for describing the viscoelastic properties of a material. The complex, storage and loss moduli, and the phase angle are illustrated by the trigonometry of a right triangle, as shown in Figure 3.3.

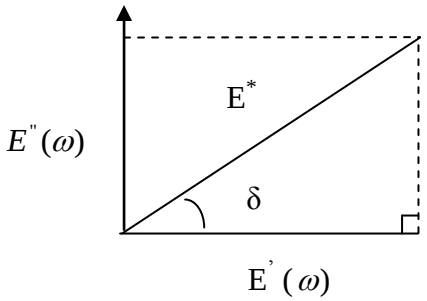

Figure 3.3: Relation among dynamic E', E'' and phase angle (Sperling, 1992).

It follows that the loss tangent can be calculated simply as the tangent of the phase angle, or alternatively, as the ratio of the loss to storage moduli:

$$\tan \delta = E'' / E' = \frac{1}{\omega\tau} \qquad (3.8)$$

and that $$E^* = [(E')^2 + (E'')^2]^{1/2} \qquad (3.9)$$

where E^*, is the ratio of the peak stress to the peak strain and reflects the total stiffness. The in-phase component of E^*, i.e. the shear storage modulus, E', represents the part of the input energy which is stored (the elastic portion). The out-of-phase component of E^*; the shear loss modulus E'', represents viscous component of it. The complex dynamic shear viscosity η^* can be obtained from E^* divided by the frequency, while the dynamic viscosity is $\eta = E'' / \omega$.

3.1.2 Temperature Dependence of the Relaxation Time

The temperature dependence of polymer properties is important as their physical and mechanical properties change as temperature changes. It is important to study the relaxation behavior of polymers, at a particular temperature for a given time period. The temperature dependence of the relaxation time provides a way of varying the temperature to bring the relaxation process within a time scale that is readily accessible. Viscoelastic behavior at short or long time periods can be predicted by extrapolation. Changes due to temperature can be described in terms of free volume or relaxation time. At temperatures below the glass transition, local chain relaxation takes place. This involves motions hindered by close presence of other molecules. For relaxation to take place a potential barrier must be surmounted. In this region the kinetics of relaxation are better described on the basis of barrier state theories. The temperature dependence of the relaxation time, τ, is often described by the Arrhenius equation shown in equation 3.10 (Sperling, 1992).

$$\tau = \tau_o \exp\left[\frac{E_a}{kT}\right] \qquad (3.10)$$

where τ_o is the pre-exponential factor, E_a is the activation energy, *k* is Boltzmann constant and *T* is the absolute temperature.

In contrast to local motions, relaxation time, τ, associated with secondary motions are dependent on free volume. The presence of volume allows the molecules to relax to a new configuration. Doolittle equation gives a relation that expresses the dependence of relaxation time on the free volume as shown in equation 3.11 (Doolittle and Doolittle, 1957).

$$\tau = \tau_o \exp\left(\frac{BV_O}{V - V_O}\right) \qquad (3.11)$$

where V is the total volume, V_o is the occupied volume, $B = \xi\left(\frac{V^*}{V_m}\right)$ is a constant, V^* is the minimum volume required for relaxation process to take place, V_m is the mean volume of the relaxing polymer segment, ξ is a constant such that $0.5 < \xi < 1$. At temperature above the glass transition (T_g), the dependence follows the William-Landel-Ferry (WLF) law (Ward and Hadley, 1993). Their relationship is illustrated by equation 3.12.

$$\log \frac{\tau(T)}{\tau(T_g)} = -\frac{C_1(T - T_g)}{C_2 + T - T_g} \qquad (3.12)$$

where $\tau(T)/\tau(T_g)$ = the shift factor relative to the reference temperature, T_g, C_1 & C_2 are empirically determined constants and T_g is a glass transition temperature. For temperatures less than the reference temperature the shift factor moves the curves to the right while for higher temperatures the curves shift to the left. The values of C_1 and C_2 depend

on the particular morphology or structure associated with a given sample. For amorphous materials, the best approximations for the parameters are C_1 = 17.44 and C_2 = 55.6. As the sample becomes more crystalline (e.g. polyethylene or the asphalt paraffins) or cross linked (such as a vulcanized rubber), the values of C_1 and C_2 will increase, reflecting changes in the free volume and the expansion with respect to temperature. Figure 3.4 shows curve comparison of VFT and Arrhenius relationships.

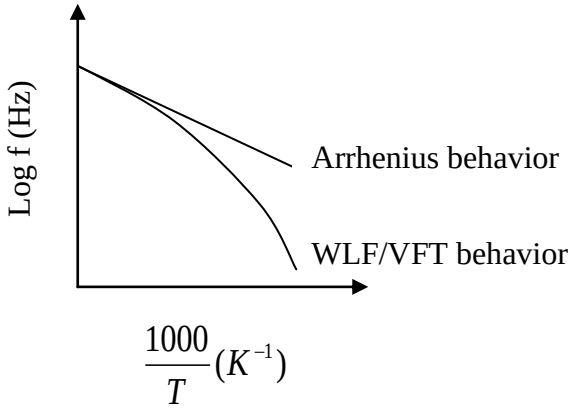

Figure 3.4: Comparison of the Arrhenious and VFT/WLF relationship (Sperling, 1992 and McCrum *et al.*, 2003)

Conversely, Vogel-Fulcher-Tamman equation (Vogel, 1921) can also be used to explain temperature dependence above T_g. The VFT equation is shown by relation of equation 3.13

$$\tau = \tau_o \exp\left[\frac{K}{T - T_o}\right] \qquad (3.13)$$

where τ_o is the characteristic time at which free volume would be zero, $K = \left(\frac{BV_O}{\alpha}\right)$ is a constant and T_o is ideal (Vogel) temperature which is 50 ^oC below T_g, temperature at which free volume would be zero.

3.2 Creep and Recovery behavior

Creep is a time- and temperature-dependent phenomenon, occurring under load control. It occurs at both high and low temperatures. For polymers, creep regime occurs above the glass transition temperature. It is a combination of behaviors of viscous liquids and elastic solids (Herrera *et al*., 2005). Creep in polymers occurs by chains untangling and slipping relative to one another; since a polymer consists of long chain-like molecules in a tangled and coiled arrangement. The concept of viscoelasticity of polymers comes from the fact that most materials do not exhibit purely elastic (ideal solids) or purely viscous (ideal liquid) behavior but a combination of both viscous and elastic in varying amounts, meaning that a polymeric system does not follow a Hookean (elastic), or viscous (Newtonian flow) behavior. Various models have been proposed to explain viscoelastic behavior. The spring element shows instantaneous elasticity due to loading and recovery due to unloading. This model fits well to purely elastic materials. Spring, which represent the elastic component of a viscoelastic material, obey Hooke's Law:

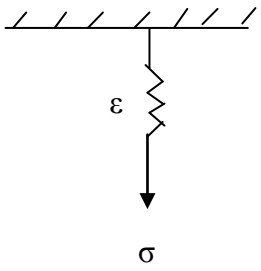

Figure 3.5: Linear spring-Elastic component (Ward and Hadley, 1993)

The constitutive equation for this element is

$$\sigma_s = E\varepsilon \qquad (3.14)$$

where σ is the applied stress, E is the creep modulus of the material, and ε is the strain. The spring represents the energetic or elastic component of the model's response. The spring element cannot be used for describing viscoelastic models like bitumen. The time dependency of viscoelastic materials are generally modelled with linear viscous dashpot. The dashpot continously deform at a constant rate when costant stress is applied. Dash-pot, which represents the viscous component of a viscoelastic material. In these elements, the applied stress varies with the time rate of change of the strain. The dash-pot arrangement can be illustrated by the sketch diagram of Figure 3.6.

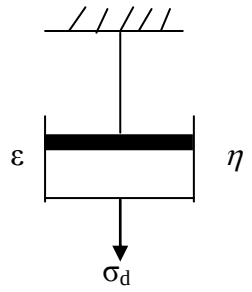

Figure 3.6: Linear dashpot-Viscous component(Ward and Hadley, 1993)

The constitutive equation of this element is

$$\sigma_d = \eta \frac{d\varepsilon}{dt} \qquad (3.15)$$

where η is viscosity of the dashpot component. Several mathematical models are developed to describe the nature of viscoelastic materials using a spring and dashpot. These include Kelvin-Voigt, Maxwell, Burgers and standard linear solid models, among others (Sperling, 1992; Smith, 2004).

3.2.1 Kelvin Model

The Kelvin–Voigt model, also called the Voigt model, can be represented by a purely viscous damper and purely elastic spring connected in parallel as shown in Figure 3.7 (a) while its creep and recovery behavior are shown in figure 3.7 (b).

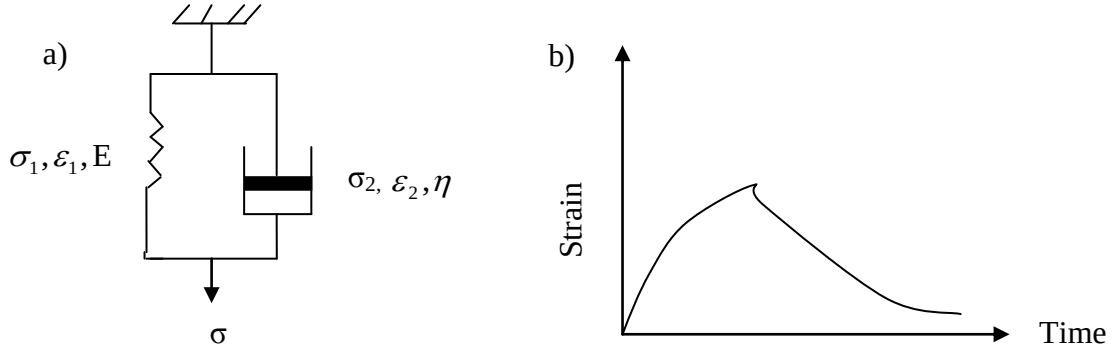

Figure 3.7: (a) Kelvin-Voigt, (b) Creep and Recovery behavior (Ward and Hadley, 1993)

Since the two components of the model are arranged in parallel, the strains in each component are identical:

$$\varepsilon_T = \varepsilon_1 = \varepsilon_2 \qquad (3.16)$$

Similarly, the total stress will be the sum of the individual stress in each component:

$$\sigma_T = \sigma_1 + \sigma_2 \qquad (3.17)$$

From these equations it can be seen that in a Kelvin–Voigt material, stress σ, strain ε and their rates of change with respect to time *t* are governed by equations of the form:

$$\sigma(t) = E\varepsilon(t) + \eta \frac{d\varepsilon(t)}{dt} \qquad (3.18)$$

where *E* is the Young's modulus of elasticity and η is the viscosity. The equation can be applied either to the shear stress or normal stress of a material. If we suddenly apply some constant stress σ_o to Kelvin–Voigt material, then the deformations would approach the deformation for the pure elastic material, σ_o / E, with the difference being the concept

of exponential decay. Equation 3.19 gives the Voigt deformation relationship.

$$\varepsilon(t) = \frac{\sigma_o}{E}(1 - e^{\frac{-t}{\tau}}) \qquad (3.19)$$

where *t* is time and τis the relaxation time, $\tau = \frac{\eta}{E_1}$

Although the Kelvin–Voigt model is effective for predicting creep, it is not good at describing the relaxation behavior after the stress load is removed.

3.2.2 Maxwell Model

The Maxwell model can be represented by a purely viscous damper and a purely elastic spring connected in series, as shown in Figure 3.8 (a). The creep and recovery behavior is shown in figure 3.8 (b).

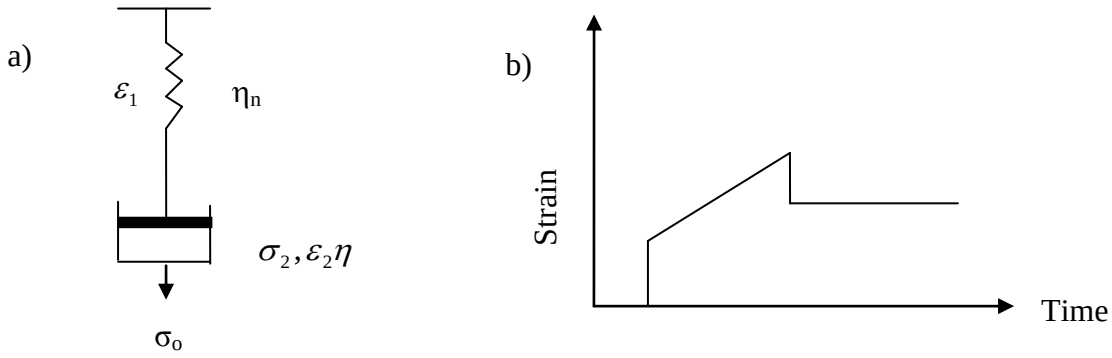

Figure 3.8: (a) Maxwell model, (b) Creep and Recovery behavior (Ward and Hadley, 1993)

The total stress, σ_T and the total strain, ε_T can be defined as shown in equation 3.20

$$\sigma_T = \sigma_1 = \sigma_2$$

$$\varepsilon_T = \varepsilon_1 + \varepsilon_2 \qquad (3.20)$$

In this model, stress σ, strain ε and their rates of change with respect to time *t* are governed by equations of the form shown in equation 3.21

$$\frac{d\varepsilon}{dt} = \frac{\sigma}{\eta} + \frac{1}{E}\frac{d\sigma}{dt} \qquad (3.21)$$

where *E* is the elastic modulus and η is the material coefficient of viscosity. If a Maxwell material is suddenly subjected to a stress σ_o, then the elastic element would suddenly deform and the viscous element would deform with a constant rate given by equation 3.22.

$$\varepsilon(t) = \frac{\sigma_o}{E} + \frac{\sigma_o}{\eta}t \qquad (3.22)$$

The Maxwell Model is not ideal for predicting the creep behavior of a material since it describes the strain relationship with time as linear (Ward and Hadley, 1993).

3.2.3 Burgers model

Burgers combines Maxwell model in series with a certain number of Kelvin-voigt models as shown in Figure 3.9 (a), is one of the most used models to give the relationship between the morphology of the blends and their creep behavior (Findley *et al.*, 2007). For linear viscoelastic solid, the total strain is the sum of three essentially separate parts: the immediate elastic deformation, the delayed elastic deformation and the Newtonian flow, which is identical with the deformation of a viscous liquid obeying Newton's law of viscosity (Findley *et al.*, 1989).

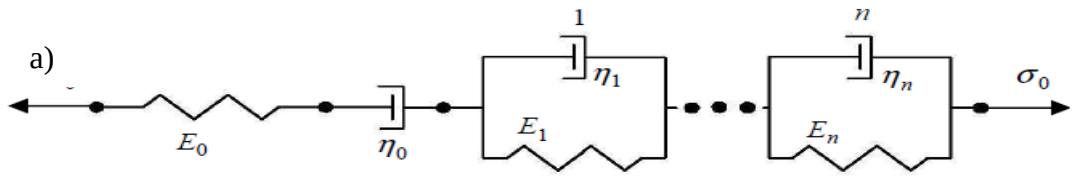

Figure 3.9: a) Generalized Burgers Model (Findley *et al.*, 1989)

b)

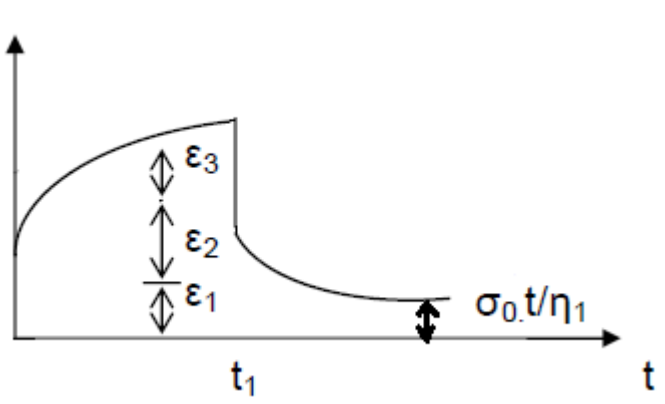

Figure 3.9: (b) creep and recovery behavior (Findley *et al.*, 1989)

Figure 3.9 (b) shows creep and recovery behavior of the Burglers model. If a constant stress is applied to the extremities of the mechanical model, because of the equilibrium, the same stress is shared by each element while the strains (and stress rates) are additive as shown in equation 3.23

$$\varepsilon(t) = \sigma\left[\frac{1}{E_o} + \frac{1}{\eta_o} + \sum_{i=1}^{n}\frac{1}{E_i}\left(1 - e^{\frac{t}{\tau_i}}\right)\right] \qquad (3.23)$$

As can be seen, parameters are necessary for completely describing the generalized burgers model, namely $E_{o,}\eta_o$, E_i and $\tau_i = \eta_i / E_i$ (i = 1,2,3….), which are, respectively, the instantaneous elastic modulus, the viscosity of the Maxwell element, delayed elastic modulus and the relaxation time of the generic i-th voigt element. The strain per unit of applied stress provides the so called creep compliance, from equation (3.23), we recognize that the generalized burgers model provides an exponential decay of the creep compliance. This is not surprising because in this model spring and dashpot yield forces that are proportional to derivatives of zero-th order (spring) and first order (dashpot)

3.2.4 Standard Linear Solid Model

The standard linear model combines a spring and a Kelvin element in series as shown in Figure 3.10.

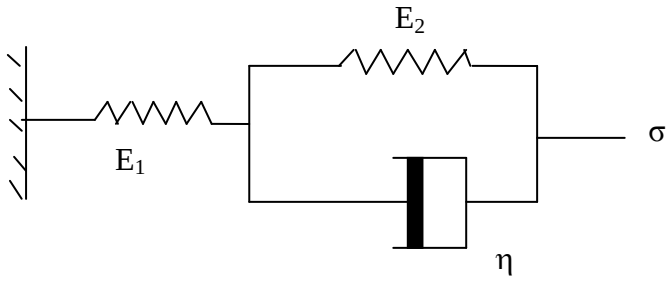

Figure 3.10: Standard Linear Solid model (Ward and Hadley, 1993)

By considering equilibrium of stress and compatibility of strains, the governing equation for this model shown in equation 3.24 (Ward and Hadley, 1993)

$$\eta E_1 \frac{d\varepsilon}{dt} + E_1 E_2 \varepsilon = \eta \frac{d\sigma}{dt} + (E_1 + E_2)\sigma \qquad (3.24)$$

For a constant stress $\sigma_{o,}$ the corresponding strain is obtained by solving equation (3.24). Since stress is a constant, $\frac{d\sigma}{dt} = 0$. Equation (3.24) becomes,

$$\eta E_1 \frac{d\varepsilon}{dt} + E_1 E_2 \varepsilon = (E_1 + E_2)\sigma \qquad (3.25)$$

this can be rewritten as shown in equation 3.26

$$\frac{d\varepsilon}{dt} + \frac{E_2 \varepsilon}{\eta} = (E_1 + E_2)\frac{\sigma}{\eta E_1} \qquad (3.26)$$

Noting that the equation has an integrating factor, $e^{\frac{E_2 t}{\eta}}$, we obtain an expression for strain as shown in equation 3.27

$$\varepsilon e^{\frac{E_2 t}{\eta}} = (E_1 + E_2)\frac{\sigma}{E_1 E_2} e^{\frac{E_2 t}{\eta}} + C \qquad (3.27)$$

At t = 0, $\varepsilon = \frac{\sigma_0}{E_1} + \frac{\sigma_o}{E_2}$ substituting these values in (3.27) and solving for C, we obtain an expression of strain as shown in equation 3.28

$$\varepsilon = \frac{\sigma_0}{E_1} + \frac{\sigma_0}{E_2}\left[1 - \exp\left(-\frac{t}{\tau}\right)\right] \qquad (3.28)$$

where $\frac{\sigma_0}{E_1}$ is instantaneous elastic deformation corresponding to the spring, $\frac{\sigma_0}{E_2}$ is delayed elastic deformation corresponding to the Kelvin element, E_1 and E_2 are elastic moduli. At t =0, $\varepsilon = \frac{\sigma_o}{E_1}$ and $\tau = \frac{\eta}{E_2}$, where η is viscosity, τ is retardation (relaxation) time, which is defined as the time take for the stress to fall to a value $\frac{1}{e} = \frac{1}{2.7}$ of the original stress. In other words it is the measure of how quickly a material recovers. This is illustrated in Figure 3.11.

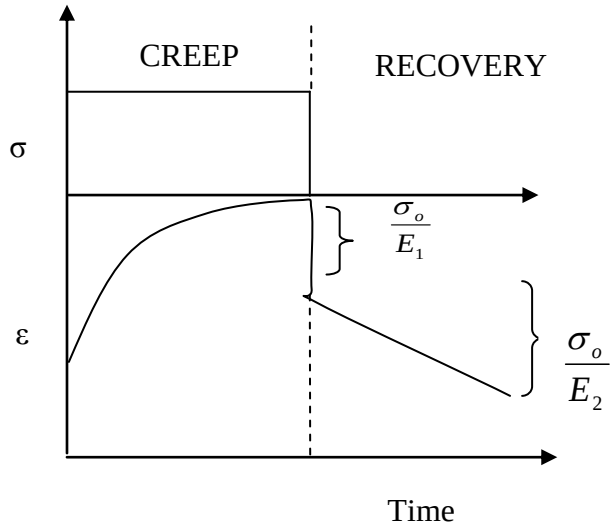

Figure 3.11: Creep response of Standard linear solid model (Ward and Hadley, 1993)

The time dependence of the relaxed moduli in the creep (C_p) and subsequent recovery(R) processes at different loading levels are given by equation 3.29

$$C_p = \frac{E_0 - E_t}{E_0} \text{ and } R = \frac{E_0^{'} - E_t^{'}}{E^{'}_0} \qquad (3.29)$$

where E_t represents the creep modulus at time t seconds, $E^{'}_t$ represents the modulus at the time t in the recovery process, E_o represents the original modulus in the creep process, and $E_o^{'}$ is the initial modulus in the subsequent strain recovery process at 10s after 3600s of creep.

3.3 Standard linear model solution for creep and relaxation

The simplest combination is shown in Figure 3.10 and consists of a Voigt model with a spring in series. If we let the modulus of the additional spring be E_1 and of the spring in the Voigt model be E_2 as shown then the differential equation is

$$\frac{d\varepsilon}{dt} + \frac{E_2 \varepsilon}{\mu} = \frac{E_1 + E_2}{\mu} \frac{1}{E_1} \sigma + \frac{1}{E_1} \frac{d\sigma}{dt} \qquad (3.30)$$

From which it can be seen that both creep and relaxation result in satisfactory relationships. The creep compliance function is expressed by equation 3.31

$$J(t) = \frac{1}{E_1} + \frac{1}{E_2}\left[1 - \exp\left(-\frac{t}{t_2}\right)\right] \qquad (3.31)$$

where $\tau_2 = \mu / E_2$ and the relaxation modulus shown in equation 3.32

$$M(t) = E_1 - \frac{E_1^2}{E_1 + E_2}\left[1 - \exp\left(\frac{-t}{\tau_1}\right)\right] \qquad (3.32)$$

where $\tau_1 = \mu/(E_1 + E_2)$

Thus adequate qualitative representations of both relaxation and creep behavior are obtained in a single model and the time parameters for the two responses, τ_1 and τ_2, are different. The forms of the functions are of interest and they are shown schematically in Figure 3.12. Both M (t) and 1/J (t) tend to E_1 as t $\rightarrow$0 and E_1 E_2/(E_1+ E_2) as t $\rightarrow \infty$ which is apparent from an inspection of the model. The curves are sigmoidal in the form and their shape depend on τ_1 and τ_2. The bulk of the change takes place over the time range where t$\approx \tau_1$ or τ_2 and thus, as $\tau_1 < \tau_2$ in this case, the M (t) curve will always be the lower of the two. This shape of curve gives rise to the concept of the short time modulus E_1 and a long time modulus E_1 E_2/(E_1+ E_2) which is sometimes used. If any attempt is to be made to fit these curves to real data then it is apparent that the fixed shape allows little flexibility.

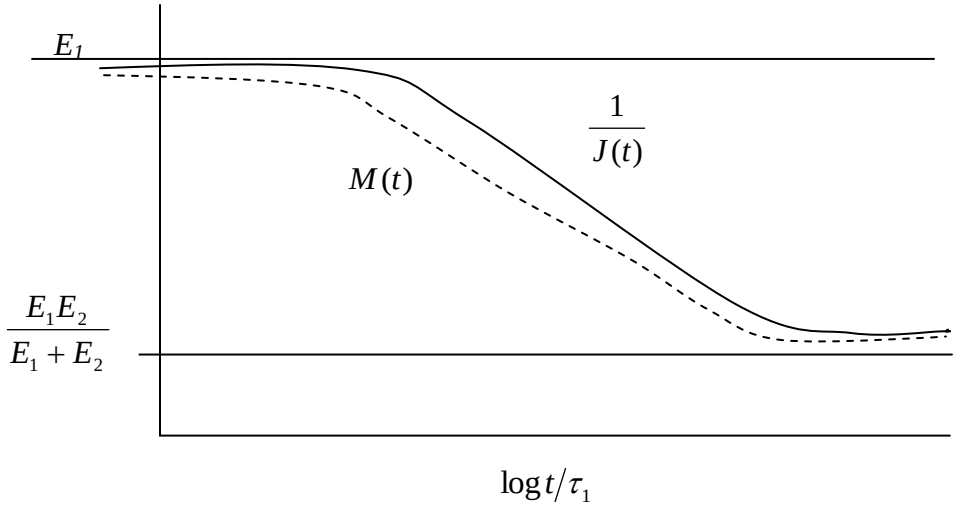

Figure 3.12: Modulus functions for the standard linear solid (Ward and Hadley, 1993).

It is therefore usual to consider models with very many elements to reproduce some shape and in general a large number of Maxwell models in parallel are used to predict relaxation behavior giving a function of the form shown in equation 3.33

$$M(t) = \sum_{i=1}^{n} E_i \exp\left(-\frac{t}{\tau_1}\right)$$

$$M(t) = \int_0^{\infty} \sum_{i=1}^{n} E(\tau) \exp\left(-\frac{t}{\tau_1}\right) d\tau \qquad (3.33)$$

This is the relaxation spectrum concept in which changes in M (t) may be linked with relaxation times within the spectrum. The long time modulus for this system tends to zero. Similarly, a set of voigt models in series gives equation 3.34

$$J(t) = \int_0^{\infty} \frac{1}{E(\tau)} \left[1 - \exp\left(-\frac{t}{\tau}\right)\right] d\tau \qquad (3.34)$$

which gives a spectrum of times for creep behavior. This approach has been commonly used in attempts to relate molecular structure to macroscopic properties, and in particular to relate the various relaxation times to identifiable molecular motions within the structure (Ward and Hadley, 1993).

Returning to the standard linear solid, we find that by using J(t) and M(t) the expression for constant stress rate and constant strain rate may be derived. For a constant stress rate this may be written in the form of a modulus shown in equation 3.35

$$E_{stress} = \frac{E_1 E_2}{E_1 + E_2} \left[\frac{1}{1 - \frac{\tau_1}{t} \frac{E_1}{E_2} \left(1 - \exp\left(-\frac{t}{\tau_2}\right)\right)} \right] \qquad (3.35)$$

and for constant strain rate:

$$E_{strain} = \frac{E_1 E_2}{E_1 + E_2}\left[1 + \frac{E_1}{E_2}\frac{\tau_1}{t}\left(1 - \exp\left(-\frac{t}{\tau_1}\right)\right)\right] \qquad (3.36)$$

Equation (3.35) and (3.36) may be written to give comparable forms:

$$E_{creep} = \frac{E_1 E_2}{E_1 + E_2}\left[\frac{1}{1 - \frac{E_1}{E_1 + E_2}\exp\left(-\frac{t}{\tau_2}\right)}\right]$$

and $$E_{relax} = \frac{E_1 E_2}{E_1 + E_2}\left[1 + \frac{E_1}{E_2}\exp\left(-\frac{t}{\tau_1}\right)\right] \qquad (3.37)$$

The four expressions give the slopes of the isochronous curves for the four systems of loading for any given value of t. All tend to the long time modulus for $t \to \infty$ but for other values of t they are in fixed order namely: $E_{relax} < E_{creep} < E_{strain} < E_{stress}$

3.4 Sinusoidal Loading

Sinusoidal loading is of considerable practical interest and it is convenient to consider it in relation to the standard linear solid. If we consider first a cyclic stress input:

$$\sigma = \sigma_o \sin \omega t \qquad (3.38)$$

where ω is the angular frequency then this function can be used together with J(t) from equation (3.31) to give the convolution integral:

$$\varepsilon(t) = \int_0^t \left[\frac{1}{E_1} + \frac{1}{E_2}\{1 - \exp\left(-\frac{t-\tau}{\tau_2}\right)\}\right]\sigma_0 \omega \cos \omega\tau d\tau$$

which may be evaluated to give equation 3.39

$$\varepsilon(t) = \sigma_o\left(\frac{1}{E_1} + \frac{1}{E_2}\frac{1}{1+\omega^2{\tau_2}^2}\right)\sin \omega t - \frac{\sigma_o}{E_2}\frac{\omega\tau_2}{1+\omega^2{\tau_2}^2}\cos \omega t + \frac{\sigma_o}{E_2}\frac{\omega\tau_2}{1+\omega^2{\tau_2}^2}\exp\left(-\frac{t}{\tau_2}\right) \qquad (3.39)$$

It can be seen that the first term may be regarded as in-phase with the sinusoidal input and the second term as out-of-phase. The third term is a transitory effect which tends to zero for long times and is usually ignored. The results are conventionally written in terms of in-phase and out-of-phase moduli designated E' and E'' respectively which in this case are:

$$\frac{1}{E^{'}} = \frac{1}{E_1} + \frac{1}{E_2}\frac{1}{1+\omega^2\tau_2{}^2} \tag{3.40}$$

and

$$\frac{1}{E^{''}} = \frac{1}{E_2}\frac{\omega\tau_2}{1+\omega^2\tau_2{}^2}$$

For high frequencies ($\omega\tau_2$>>1), E'$\rightarrow$E$_1$ and E''$\rightarrow\infty$ while for low frequencies ($\omega\tau_2$<<1), E'$\rightarrow$E$_1$ E$_2$/ (E$_1$+E$_2$) and E''$\rightarrow\infty$. Again an inspection of the model confirms these results. A further parameter of practical importance is the loss factor written as:

$$\tan\delta = \frac{\text{Out-of-phase component}}{\text{In-phase component}}$$

which in this case becomes equation 3.41

$$\tan\delta_1 = \frac{E_1\omega\tau_2}{(E_1+E_2)+E_2\omega^2\tau^2} \tag{3.41}$$

Two special cases of interest are the Maxwell model with E$_2$ = 0 and hence:

$E' = E_1, E^{''} = \omega\mu$ and the voigt model with E$_1$ = ∞ giving:

$$E^{'} = E_2(1+\omega^2\tau_2{}^2),\ E^{''} = E_2\frac{1+\omega^2\tau_2{}^2}{\omega\tau_2}$$

If the input is of the form of equation 3.42

$$\varepsilon = \varepsilon_o \sin\omega t \tag{3.42}$$

which may be regarded as strain cycling compared with stress cycling used previously, then M(t), equation (3.32), must be used in convolution integral and the results become:

$$\sigma(t) = \varepsilon_o \frac{E_1 E_2}{E_1 + E_2}\left(1 + \frac{E_1}{E_2}\frac{\omega^2\tau_1^{\,2}}{1+\omega^2\tau_1^{\,2}}\right)\sin\omega t + \varepsilon_o \frac{E_1^{\,2}}{E_1 + E_2}\frac{\omega\tau_1}{1+\omega^2\tau_1^{\,2}}\cos\omega t$$
$$-\frac{\varepsilon_o\omega\tau_1}{1+\omega^2\tau_1^{\,2}}\frac{E_1^{\,2}}{E_1 + E_2}\exp\left(-\frac{t}{\tau_1}\right)$$

As before, for long times the third term tends to zero and we have equation 3.43

$$\left.\begin{aligned} E' &= \frac{E_1 E_2}{E_1 + E_2}\left(1 + \frac{\omega^2\tau_1^{\,2}}{1+\omega^2\tau_1^{\,2}}\frac{E_1}{E_2}\right) \\ E'' &= \frac{E_1^{\,2}}{E_1 + E_2}\frac{\omega\tau_1}{1+\omega^2\tau_1^{\,2}} \end{aligned}\right\} \qquad (3.43)$$

As would be expected from the difference in creep and relaxation moduli, the moduli from stress cycling and from strain cycling are different. For example, if both expression for E' are written in terms of τ_1, we have, from equations (3.43)

$$E'_{strain} = \frac{E_1 E_2}{E_1 + E_2}\left[1 + \frac{\omega^2\tau_1^2}{1+\omega^2\tau_1^2}\frac{E_1}{E_2}\right]$$

and from equations (3.39):

$$E'_{stress} = \frac{E_1 E_2}{E_1 + E_2}\left[1 + \frac{\omega^2\tau_1^2}{\frac{E_2}{E_1+E_2}+\omega^2\tau_1^2}\frac{E_1}{E_2}\right] \qquad (3.44)$$

The only difference is in the term $E_2/(E_1 + E_2)$ and clearly $E'_{strain} < E'_{stress}$ as expected. The two expressions are shown plotted in Figure 3.12 as a fraction of $\log 1/\omega\tau_1$ and for low frequencies, $\omega\tau_1 \ll 1$, both tend to a value of $E_1E_2/(E_1 + E_2)$ which corresponds to the long time response as shown in Figure 3.13 for other histories. Similarly at high frequencies, i.e. short times, both tend to a value of E_1. The loss factor is given by:

$$\tan\delta_2 = \frac{E_1\omega\tau_1}{E+(E_1+E_2)\omega^2\tau_1^2} = \frac{E_1\omega\tau_2\frac{E_2}{E_1+E_2}}{E_2+(E_1+E_2)\omega^2\tau_1^2\frac{E_2^2}{(E_1+E_2)^2}} = \tan\delta_1$$

Thus the loss factor expression is the same for both types of loading and is shown in Figure 3.13. At both high and low frequencies it tends to zero and there is a maximum of:

$$\tan\delta = \frac{1}{2}\frac{E_1}{E_2}\sqrt{\frac{E_2}{E_1+E_2}} \qquad (3.45)$$

$$\omega\tau_1 = \sqrt{\frac{E_2}{E_1+E_2}} \qquad (3.46)$$

The special cases for strain cycling are: for the Maxwell model$(E_2 = 0)$

$$E' = E_1\frac{\omega^2\tau_1^2}{1+\omega^2\tau_1^2}, E'' = E_1\frac{\omega\tau_1}{1+\omega^2\tau_1^2}$$

and for the voigt model $(E_1 = \infty)$ $\qquad E'' = E_2,\ E'' = \omega\mu$

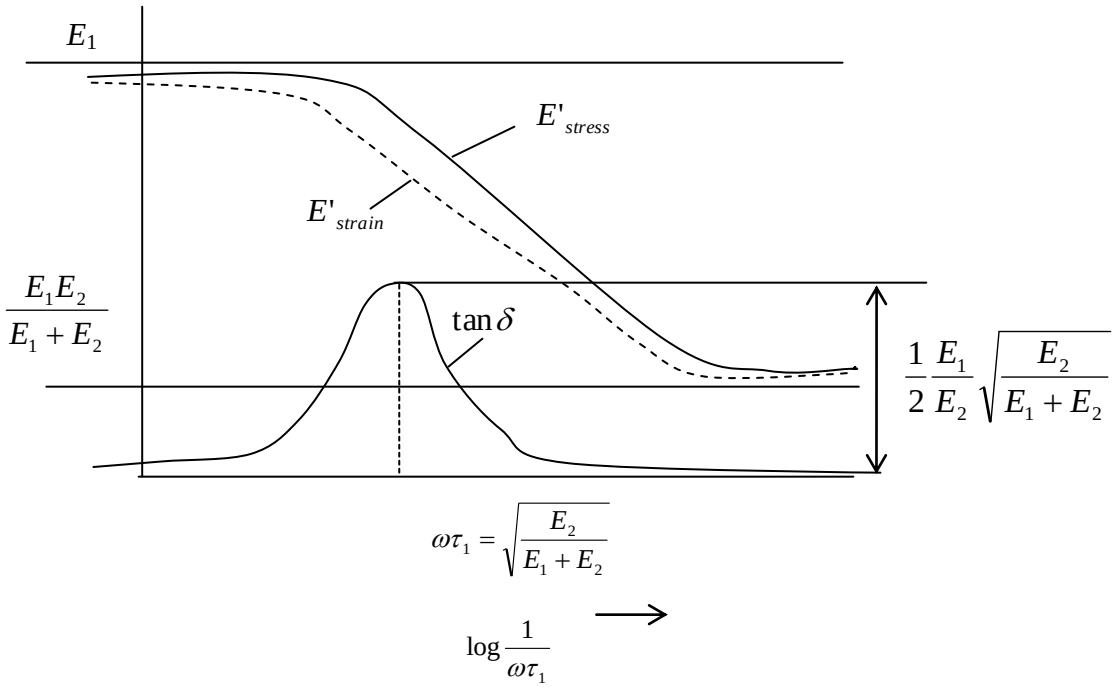

Figure 3.13: Sinusoidal loading of a standard linear solid (Ward and Hadley, 1993).

The result for the Maxwell model is used to define relaxation spectra from E' and E'' as functions of ω in a similar manner to creep and relaxation data so that:

$$E' = \int_0^\infty E(\tau)\frac{\omega^2\tau^2}{1+\omega^2\tau_1^2}d\tau \text{ and } E'' = \int_0^\infty E(\tau)\frac{\omega\tau}{1+\omega^2\tau^2}d\tau \quad (3.47)$$

3.5 Diffusion

Fick's first law according to Smith (2004) relates the diffusive flux to the concentration field as shown by equation 3.48.

$$J = -D\frac{\partial C}{\partial x} \quad (3.48)$$

where J is the diffusive flux, C is the concentration, D is the diffusion coefficient, and x is the position. If a plane polymer sheet is exposed to a fluid the change in concentration (C) of a diffusing substance as a function of time, t and position, x is given by Fick's second law (Fugita, 1968 and Crank, 1975):

$$\frac{\partial C}{\partial t} = D\frac{\partial^2 C}{\partial x^2} \quad (3.49)$$

$$\frac{\partial C}{\partial t} = -\frac{\partial}{\partial x}J = \frac{\partial}{\partial x}(D\frac{\partial}{\partial x}C) \quad (3.50)$$

Assuming the diffusion coefficient D to be a constant (J is the diffusion flux) we can exchange the orders of the differentiating and multiplying by the constant:

$$\frac{\partial}{\partial x}(D\frac{\partial}{\partial x}C) = D\frac{\partial}{\partial x}\frac{\partial}{\partial x}C = D\frac{\partial^2 C}{\partial x^2} \qquad (3.51)$$

If diffusion is restricted to one dimension, such as in the case presented by a thin film of thickness (h), absorbing a fluid according to Fick's law, where diffusion into the edges of the film can be ignored, the amount of diffusant, (M), taken up by the sheet in a time (t) can be given by equation 3.51 (Devi *et al.*,1997). The solution of equation 3.49 is:

$$\frac{C - C_0}{C_{\max} - C_0} = 1 - \frac{4}{\pi}\sum_{n=0}^{\alpha}\frac{(-1)^n}{2n+1}\exp[-D(2n+1)^2\pi^2 t/h^2\cos\frac{(2h+1)\pi x}{h}\ ] \qquad (3.52)$$

where C_0 is diffusant's concentration and the surface is kept at a constant concentration $C_{\max}$. Figure 3.13 shows the relation between $M/M_{\max}$ and time. Equation 3.52 can be written as

$$\frac{M}{M_{\max}} = 1 - \frac{8}{\pi^2}\sum_{n=0}^{\infty}\frac{1}{(2n-1)^2}\exp[-D(2n+1)^2\pi^2 t/h^2] \qquad (3.53)$$

where $M_{\max}$ is the maximum quantity of the diffusing substance at infinite time. The uptake is considered to be a diffusion process controlled by a constant diffusion coefficient, D, and $M_{\max}$ is the equilibrium sorption attained theoretically after infinite time. Equation 3.52 also describes desorption from the same sheet, initially controlled to a uniform con-

centration, whose surface concentration are instantaneously brought to some lower value or zero at t=0.

The value of *D* can be deduced from an observation of the initial gradient of a graph of M/M_{max} as a function of $\left(t/h^2\right)^{1/2}$. This observation is made easier by the fact that, for a constant diffusion coefficient, the initial part of the graph for a sorption experiment is a straight line, to within the normal limits of experimental error as shown in Figure 3.14 (Ramazan *et al.*, 2007).

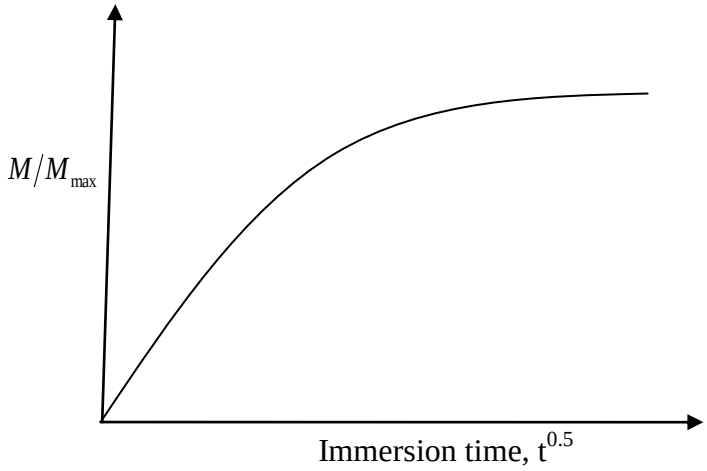

Figure 3.14: M/M_{max} against time (Ramazan *et al.*, 2007)

A simplified form of equation 3.53 has the form shown in equation 3.54

$$\frac{M}{M_{max}} = 4\left[\sqrt{\frac{Dt}{\pi h^2}}\right] \qquad (3.54)$$

For polymeric analysis equation 3.54 is a valid representation of the time dependence of the water uptake (David *et al.*, 1996). Although analytical methods for obtaining expres-

sions for the sorption rate from Fick's equations are not possible when *D* is a function of the concentration, equation 3.54 can be used as an initial sorption law. It turns out, however, that equation 3.54 holds up to higher values of M/M_{max} when the diffusion coefficient increases with concentration, whereas for *D* decreasing with increasing concentration, M/M_{max} is only proportional to $t^{1/2}$ over the very initial region of the sorption (Ramazan *et al.*, 2007).

3.6 Thermal degradation

3.6.1 Degradation kinetics

Thermal degradation is a process where the action of heat or elevated temperatures on a material causes a loss of physical, mechanical or electrical properties (Beyer and Marcelo, 2009). It is studied using Thermogravimetric Analyzer (TGA) where a sample is heated in a controlled atmosphere at a defined heating rate while simultaneously the sample mass is measured. When a polymer sample degrades, its mass decreases due to production of gaseous products like carbon dioxide, carbon monoxide and water vapour. For the very general reaction

$$S(s) = P_1(s) + P_2(s) \tag{3.55}$$

The disappearance rate of the species (S) can be calculated as follows:

$$\frac{dx}{dt} = kf(x) \tag{3.56}$$

$$x = \frac{m_o - m}{m_o - m_\infty} \tag{3.57}$$

With m is mass remaining at time t, m_o is initial mass and m_∞ is final mass. The overall kinetic equation in terms of the conversion factor, x is given by equation (3.58).

$$\frac{dy}{dt} = A(x)^n \exp\left(\frac{-E_a}{RT}\right) \tag{3.58}$$

A is a pre exponential factor, R is universal gas constant, T is the Absolute Temperature and n is the order of reaction. If the temperature of the sample is changed by a constant heating rate $\beta = \frac{dT}{dt}$ the variation in the conversion factor can be analyzed as a function of temperature, this temperature depending on the time of heating. Thus, the reaction rate is defined as:

$$\frac{dy}{dt} = \frac{A}{\beta}(x)^n \exp\left(\frac{-E_a}{RT}\right) \tag{3.59}$$

Broido (1969) derived a non-integral equation (3.60) valid only for the first order reaction.

$$\ln(\ln\frac{1}{x}) = \frac{-E}{RT} + \ln\frac{RZT_m^2}{E_a\beta} \qquad \text{for n=1} \tag{3.60}$$

Z is the frequency factor and T_m is the temperature of the maximum reaction rate.

3.7 Biodegradation

Microbial degradation results from the action of naturally occurring microorganisms such as bacteria, fungi, algae, etc. The production of biodegradable plastics that get decomposed completely in nature have received remarkable attention globally as they are totally ecofriendly and helpful in waste landfill management. Addition of natural polymers like CEL to thermoplastics having long-term potential is one of the approaches to enhance biodegradability (Dave *et al.*, 1997). To prepare biodegradable plastic involves adding special additives to the synthetic polyolefins, which make it susceptible to microbial degradation, and these additives also disconnect the continuity of C-C chain of polyolefin.

Few additives having hydrophilic groups make plastics hydrophilic and susceptible for photo- and chemical degradation.

Biodegradation is the transformation of a substance into new compounds through actions of microorganisms such as bacteria. RLDPE are inert materials not susceptible to the microbial attack because their hydrophobic backbones consisting of long carbon chains that gives high resistivity against hydrolysis, addition of antioxidants and stabilizers during their manufacture which keeps it from atmospheric oxidation and high molecular weight (Zheng and Yanful, 2005).

3.7.1 Overview of biodegradation of polymers

Polymeric materials released into the environment can undergo physical, chemical and biological degradation or combination of all these due to the presence of moisture, air, temperature, light (photo-degradation), high energy radiation (uv, γ-radiation) or microorganisms (bacteria or fungi). The rates of chemical or physical degradation are higher when compared to that of biodegradation. Also physical and chemical degradation and complete mineralization of the polymer happens due to biodegradation, which is generally the last step.

Figure 3.15 shows degradation of RLDPE which may take hundreds of years (Kawai *et al.*, 2002). Photo oxidation is the triggering step in the oxidation degradation of RLDPE. UV radiation leads to radical formation, followed by the absorption of oxygen resulting in end products with carbonyl groups. Additional UV exposure causes carbonyl group to

undergo degradation which leads to the cleavage of C-C bond and thus leading to the formation of oxidized low molecular weight fragments. Ultimately, photo oxidation leads to the formation of low molecular weight fragments and thus increases the hydrophilicity of RLDPE. Thus photo oxidation enhances susceptibility of the RLDPE to microbes. The carbons enter the β- oxidation pathway as shown in scheme 3.1. Later, the two carbon acetyl CoA, enters the TCA cycle and gets completely converted into carbon dioxide and water (Arutchelvi *et al.*, 2008). Figure 3.15 shows an overview of degradation of RLDPE.

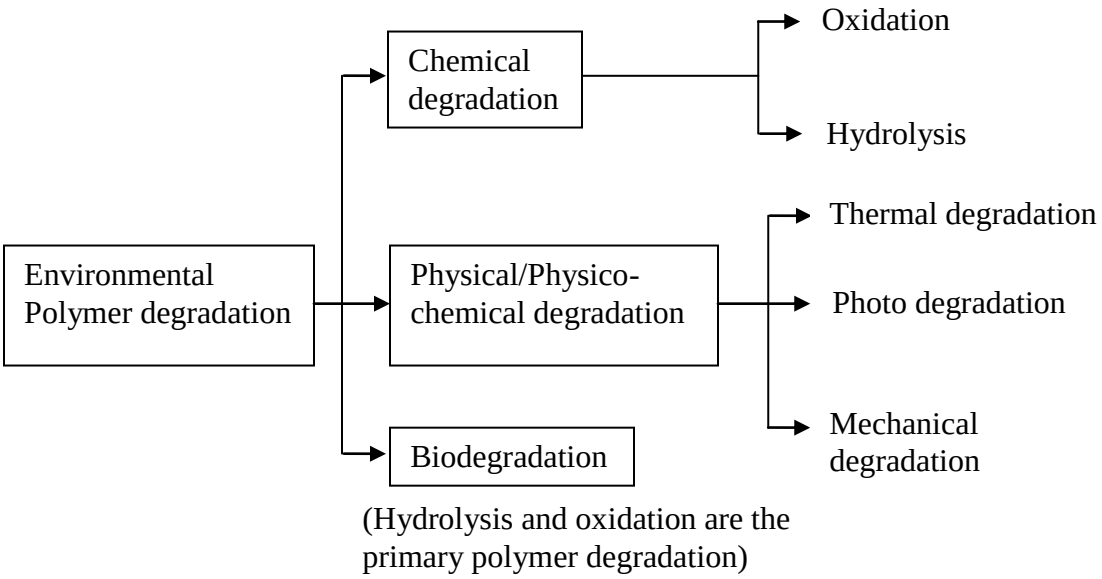

Figure 3.15: Overview of degradation of RLDPE (Arutchelvi *et al.*, 2008).

Natural soil is used to burry dried sheets of the RLDPE-CEL samples hence act as the environment for the biodegradability test. Weight loss (W_{loss}) of the degraded sheets can then be calculated using equation 3.61.

$$W_{loss} = \left[\frac{(W_b - W_a)}{W_b} \right] \times 100\% \qquad (3.61)$$

where W_b and W_a are the weights of the dried sheets before and after being buried in soil, respectively (Rui *et al*., 2006). The experimental data of biodegradation can be fitted and explained using regression lines.

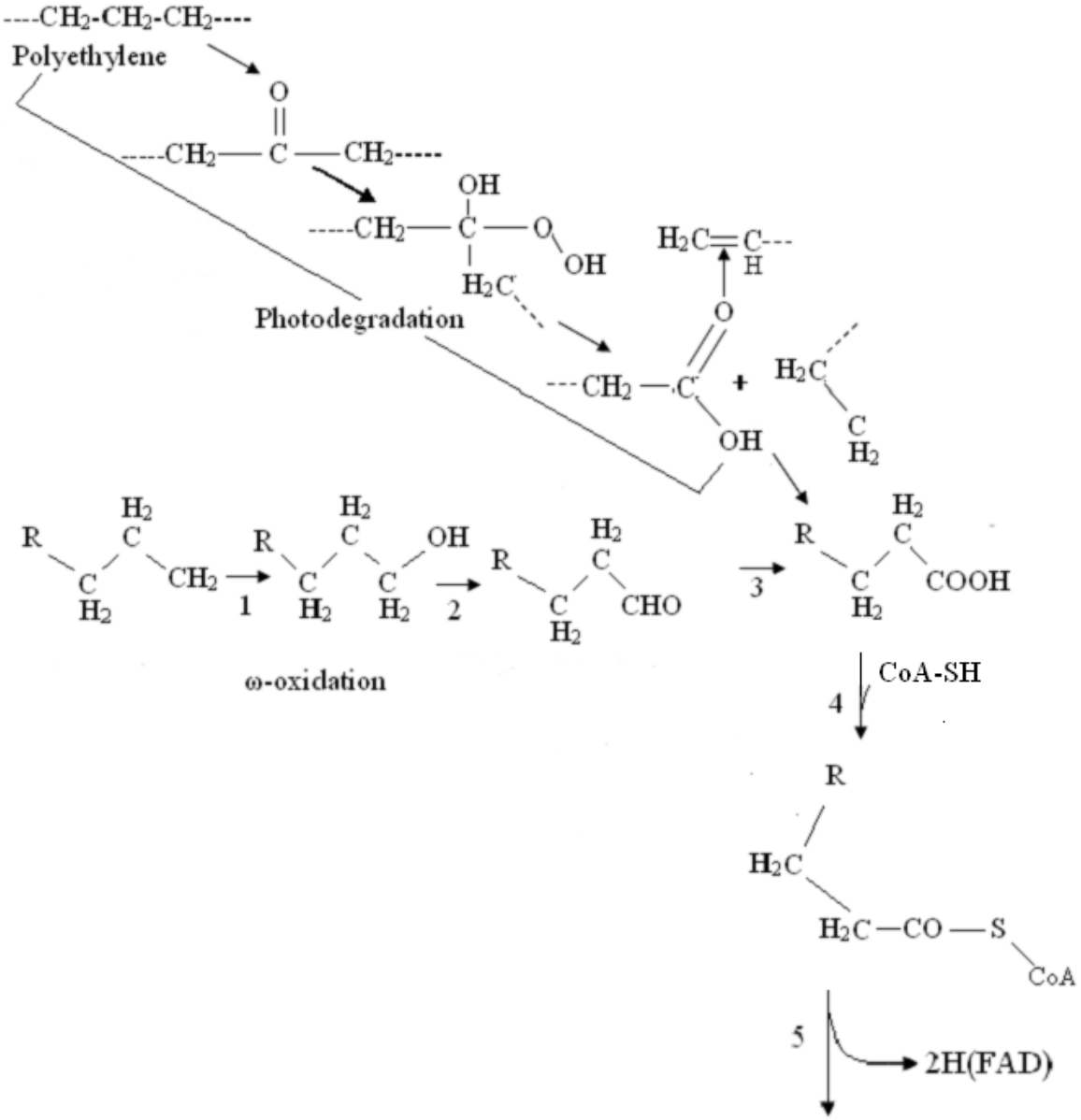

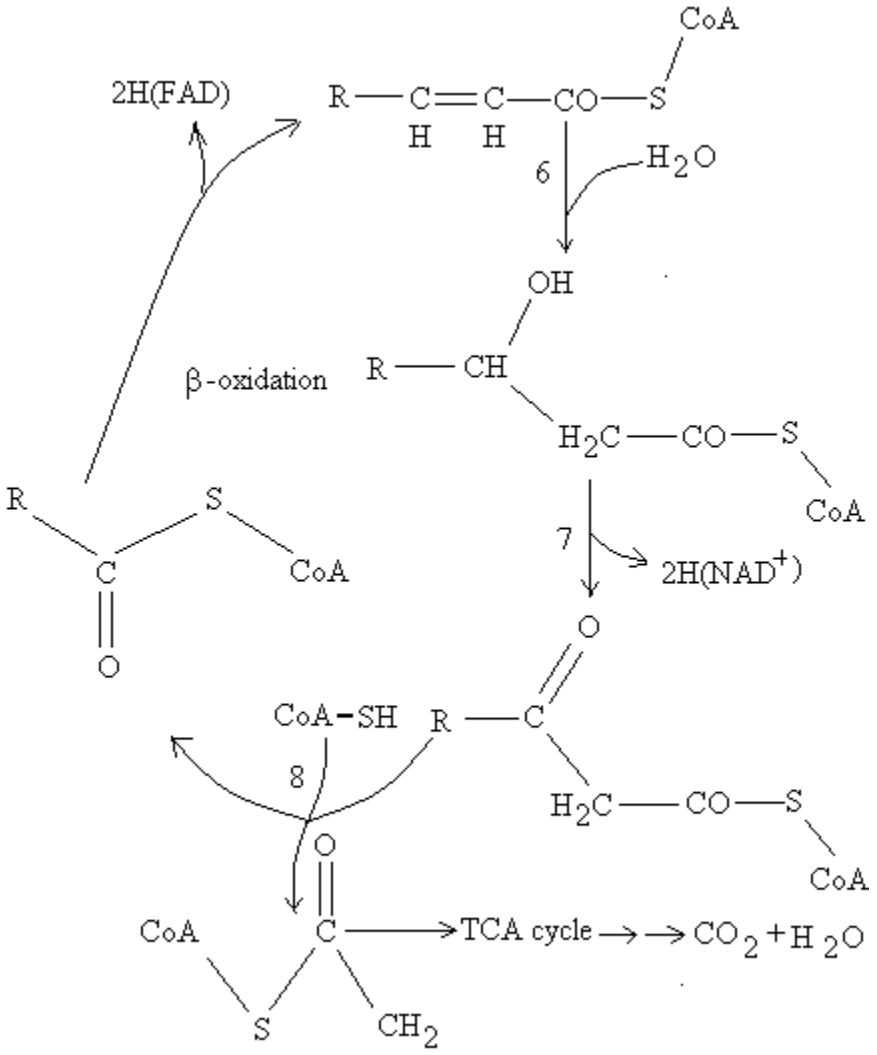

Scheme 3.1: Mechanism of biodegradation of RLDPE (Arutchelvi *et al.,* 2008)

CHAPTER FOUR

MATERIALS AND METHODS

4.1 Introduction

This chapter describes the materials, sample preparation, apparatus used for sample blending and experimental procedures adopted for DMA, diffusion and degradation measurements.

4.2 Materials

RLDPE in chips form and gray in colour was obtained from Kenplast Plastic Company in Nairobi. RLDPE has a structure that consists of a linear repeating unit $(-CH_2- CH_2-)_n$ (Cowle, 1991), where n is the number of repeating units forming the polyethylene

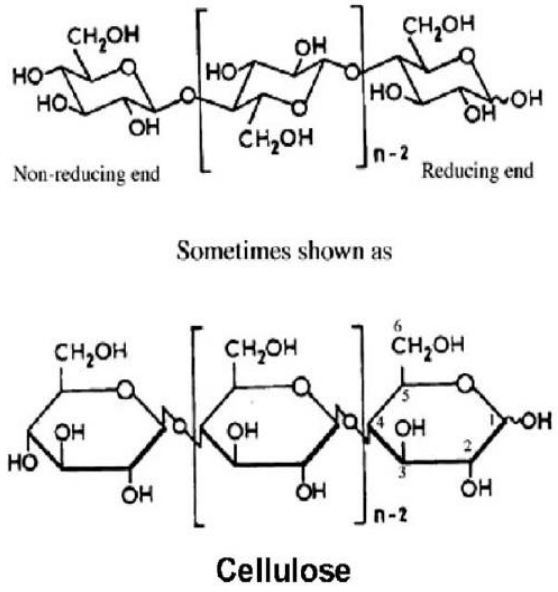

Figure 4.1: Molecular structure of CEL (Sinha and Bousmina, 2005)

chain. CEL was extracted from cell sap of Acacia (Taveta) plant. CEL has a structure that consists of a linear repeating monomer unit as shown in figure 4.1, where n again is the

number of repeating units in the CEL matrix. Table 4.1 shows some typical properties of RLDPE and CEL.

Table 4.1: Typical properties of CEL and RLDPE.

PROPERTY	CEL	RLDPE	REFERENCE
Tensile strength (MPa) (At Room Temp)	17.8	8-12	Meyers and Chawler, (1999) Kahovec and Hatada, (2002)
Molecular formula	$(C_6H_{10}O_5)$ n	$(-CH_2- CH_2-)_n$	Nishino, (1995) Cowle, (1991)
Young's modulus (At Room Temp)	150 Gpa	200-400 MPa	Levchik and Weil, (2006)
β-Transition temp T_β (^OC) α-Transition temp T_α (^OC)	-	-11 30	Levchik and Weil, (2006)
Melting temp, (^OC)	-	125-136	Shotyk *et al* (2006)
Molecular mass	-	10,000- 40,000	Arutchelvi, *et al* (2008)

4.3 Sample preparation

4.3.1 Mold

Figure 4.2 shows the top and side views of the mold used. The mold used to prepare the samples was locally made at the Kenyatta University Science Workshop. It consisted of two thick aluminium plates each measuring 150 mm by 150 mm with a non-stick coating

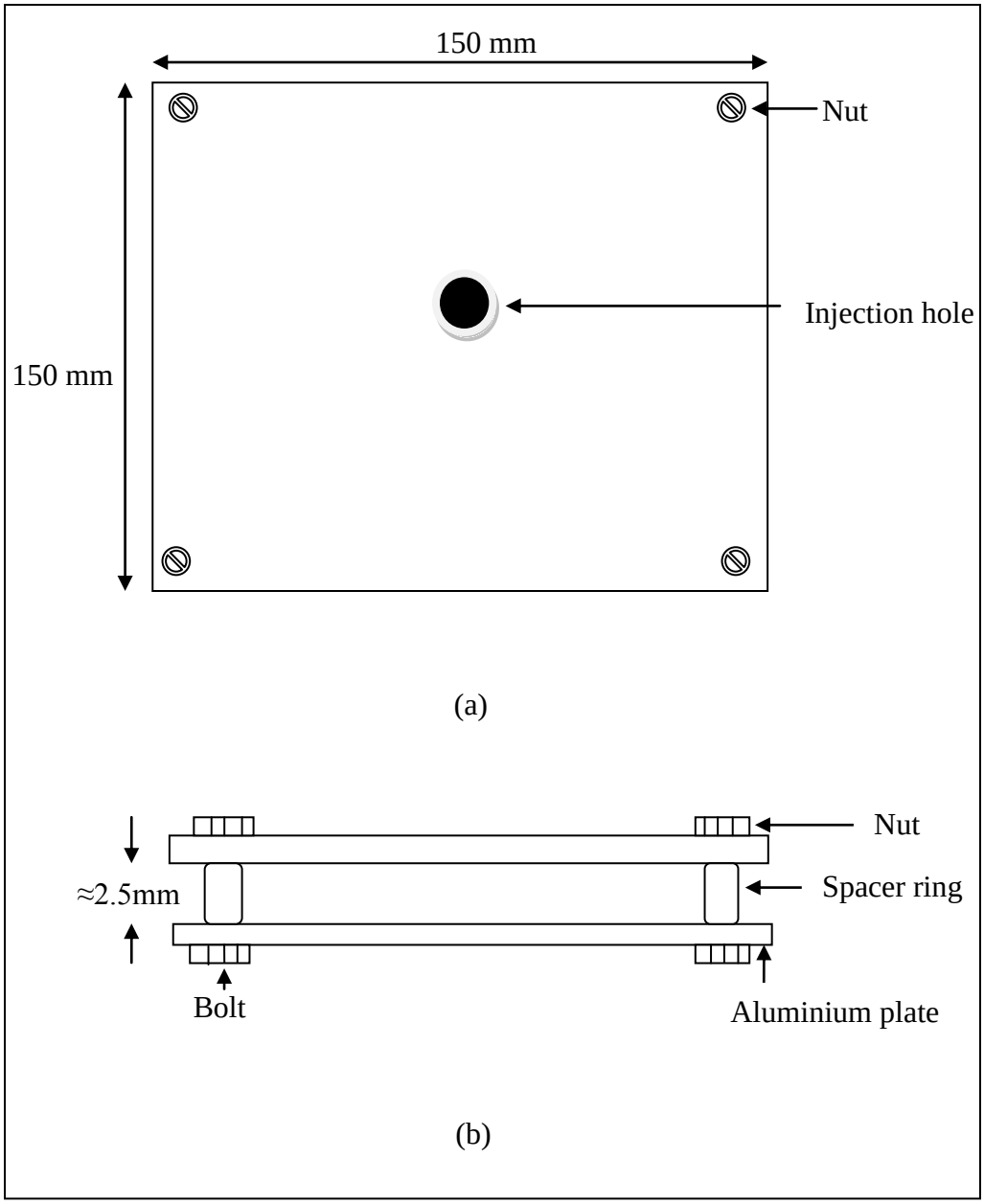

Figure 4.2: Mold; (a) top view (b) side view

on the inner surfaces of the mold. The mold also had four holes on all the corners where fastening screws were fitted. In addition the mold had four identical rings of 2 mm in thickness and an outer diameter of 10 mm. The rings acted as spacers for the aluminium

plates, and they were held in position by the fastening screws. This made it possible to obtain polymer molds of even thickness. The mold also had a 5mm diameter hole at the center of one of the plates, where the injection of the polymer melt was done.

4.3.2 Injection Machine

The injection molding process was carried out using the set up shown in Figure 4.3 below.

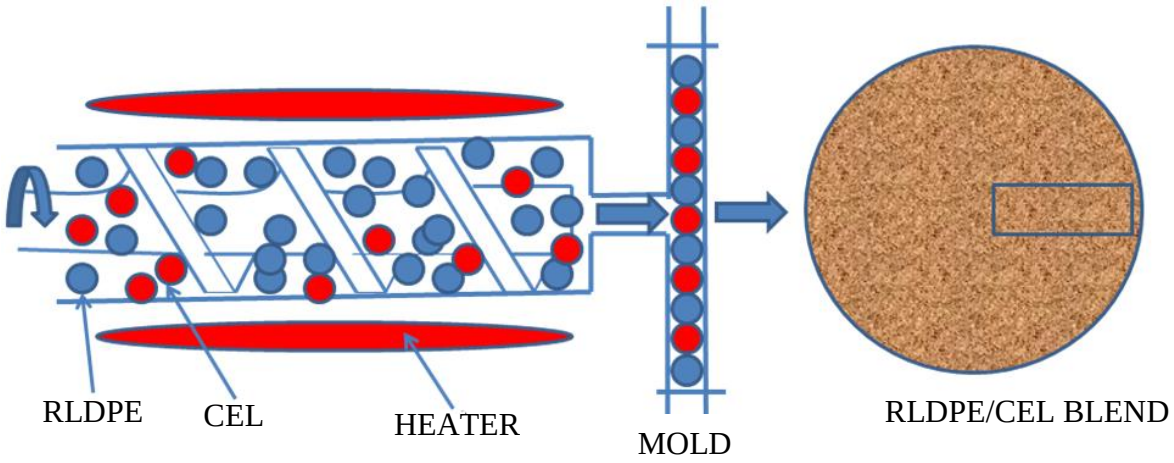

Figure 4.3: Injection moulding process.

The injection machine consisted of a cylindrical melting chamber made from brass. It had a length of 168 mm and diameter of 18 mm. It was open on one end but the other end was closed leaving a 5 mm diameter hole from where injection of the polymer melt was done. A stopper screw to fit into the hole was used during the heating process and removed just before the polymer melt was injected into the mold. The machine had a removable screw that was used for mixing the melt to homogenize the blends' mixture. It also had a piston

that fitted on the open end of the melting chamber that was used to push the polymer melt through the small hole into the mold.

4.3.3 Sample molding

Acacia cell sap was dried at 90 ^{o}C using an electric heater for 12 hours to remove the water vapour. It was then ground into a fine powder and separated with a sieve of gauge one. Mass of 10 g of RLDPE in granule form was heated at a temperature of 130 ^{o}C in the melting chamber for 30 minutes. The opening end of the chamber was closed by a stopper screw. After the RLDPE had melted CEL was carefully added and the blend was thoroughly mixed to ensure homogeneous blend. Mixtures of RLDPE-CEL were obtained in percentage ratios of 100:0, 95:5, 90:10, 85:15 and 80:20. The mixture thus prepared was stirred to ensure there is homogeneity. The stopper screw was removed and the blend mixture quickly injected through the injection hole into the disc mold as shown in Figure 4.3. The mold was then allowed to cool at room temperature for 10 minutes. When cool, the mold took the shape of the disc as shown in Figure 4.3.

The dimensions of the samples cut were 25 mm x4 mm x2 mm for mechanical measurement and 10 mm $\times 5$ mm $\times 2$ mm for diffusion and biodegradation measurements as shown in figure 4.3. All the samples thus prepared were kept in a vacuum desiccator to avoid moisture absorption. After every sample preparation procedure, the screw, piston and melting chamber were thoroughly cleaned using talc.

4.4 Measurements

4.4.1 Dynamic mechanical analysis measurement procedure

Dynamic mechanical testing was done using DMA 2980 TA instrument in the DMA Multi-Frequency - Single Cantilever mode on film samples of about 25 mm x 4 mm x 2 mm that were cut from the blend samples of RLDPE-CEL. The DMA equipment (TA instruments DMA 2980) was calibrated according to the manufacturers' recommended procedures as outlined in the user's manual. The instrument parameter was set at 0.44 and data sampling at an interval of 2.0 sec/point. In this case the instrument parameter refers to the Poisson's ratio, which is a DMA parameter that defines the ratio of transverse contraction per unit dimension to the elongation per unit length when a sample is subjected to tensile strength.

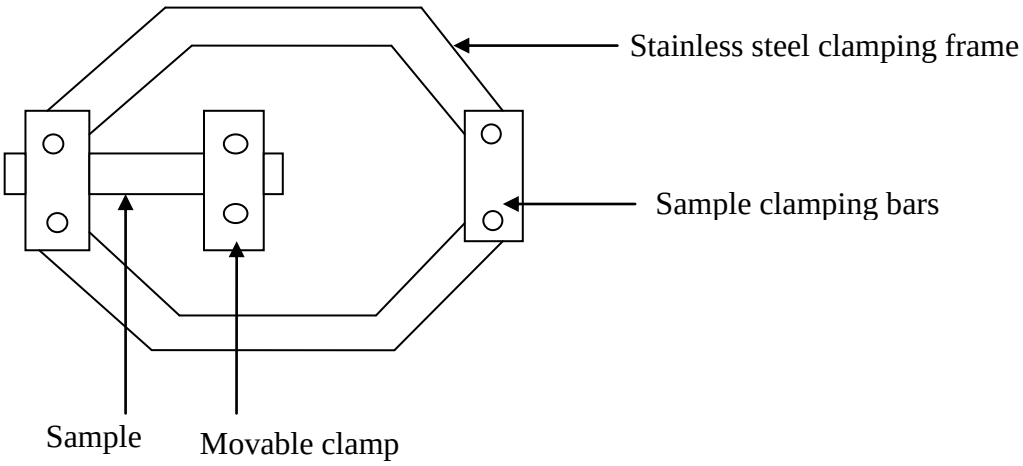

Figure 4.4: Top view of a single cantilever clamp

The storage and loss moduli were recorded in a DMA multi-frequency single cantilever mode system in the frequency range of 1 to 30 Hz, in the temperature range -30 to 90 ^{o}C and with a heating rate of 5 ^{o}C/ min. It is worth noting that the cantilever bending is used for solid samples of moderate stiffness, hence the temperature of the sample cannot be

allowed to reach its crystalline melting temperature. The sample was clamped as shown in Figure 4.4. After this, measurement started. It took about 3 hours to run a measurement.

4.4.2 Creep measurement

The creep and recovery behavior of the polymer blends were evaluated using DMA 2980 in a multi-frequency single cantilever mode at a constant span of 12 minutes. A sample of dimension 25 mm x 4 mm x 2 mm was clamped as shown in Figure 4.4. The oven was set to a desired temperature and the sample was allowed to equilibrate for 12 minutes. Subsequently, a contact pressure of 100 Pa was placed on the sample. The creep measurements were initiated by setting the machine to displace at 1 MPa, equilibrate for 20 minutes at 30 °C, 40 ^{o}C, 50 °C and 60 °C. The time of application of force was 12 minutes and the recovery time was also 12 minutes.

4.4.3 Diffusion

Blended sheets for the water diffusion tests were molded using the injection molding machine. The molded specimens (10 mm $\times$5 mm $\times$2 mm) of each composition were dried in an oven for 6 hours at a temperature of 50 $\pm$ 3 °C, cooled in a desiccators and immediately weighed until the consecutive weights were equal. The samples were placed in distilled water at room temperature (25 $\pm$ 2 °C) for 77 days. At time intervals of seven days, the test specimens were removed from the test liquid one at a time, gently blotted with tissue paper to remove the excess of water on the surface, and weighed to the nearest

0.0001 g immediately using an analytical balance. The samples were placed back in water after each measurement. The weighing was repeated at the end of every week and the average of three values was recorded. The difference between the saturated weight and the dried weight was calculated as the water absorption. The percentage gain at any time t, *%wt* as a result of moisture absorption, was determined by Equation 4.1:

$$\%Wt = \left[\frac{(W_w - W_d)}{W_d} \right] \times 100\% \qquad 4.1$$

where W_d and W_w denote weight of dry material (the initial weight of materials prior to exposure to the water absorption) and weight of materials after exposure to water absorption respectively. The equilibrium or maximum moisture absorption, W_m, was calculated as an average value of several consecutive measurements that showed no appreciable additional absorption. The weight gain resulting from moisture absorption can be expressed in terms of the diffusion coefficient or diffusivity, *D*, using equation 3.54.

4.4.4 Thermal degradation

The thermogravimetric analysis was conducted in order to assess the thermal stability of the recycled LDPE-CEL samples in percentage ratios of 100:0, 95:5, 90:10, 85:15 and 80:20. The TGA measurements were carried out on 0.0105 g of each recycled LDPE-CEL blend sample piece by monitoring the mass loss after every 5 ^{o}C at a heating rate of 5 ^{o}C/ min within a temperature range of 25 ^{o}C - 550 ^{o}C using a thermogravimetric analyzer (Model Lindberg / Blue tube furnace) in oxygen atmosphere. The kinetic parameters were obtained using equation 3.60.

4.4.5 Biodegradability

The soil burial test was an outdoor experiment that provided a realistic environment with seasonal changes, less control of soil wetness and temperature, and the presence of macro-organisms. The recycled LDPE-CEL samples in percentage ratios of 100:0, 95:5, 90:10, 85:15 and 80:20 weighing 0.15 g each were dried in an oven for 6 hours at a temperature of 50 ± 1 °C until a constant mass was obtained. The samples were then buried 20 cm beneath the ground to examine their biodegradability. This depth was chosen since it is within top soil in the soil profile where microorganisms are most active. A control box that contained only samples and no soil was also maintained for comparative studies. The moisture content was at 20-50 % of the soil's maximum water holding capacity. The soil pH was measured as 6.4. The samples were removed from the soil every 7 days. After removal, samples were washed in distilled water and dried at 50 ± 3 °C until a constant mass was obtained. The model equation $y=mx+c$ was used to fit the experimental data.

CHAPTER FIVE

RESULTS AND DISCUSSIONS

5.1 Introduction

This chapter gives the experimental results obtained from the storage and loss modulus, creep, diffusion, TGA and soil burial test. In particular the effects of CEL concentration on storage modulus, relaxation processes, creep modulus, diffusion coefficient, activation energy for thermal degradation and biodegradation of RLDPE are discussed. Both creep and DMA results are an expression of the intrinsic material's viscoelasticity and are comparable.

5.2 DYNAMIC MECHANICAL ANALYSIS

Dynamic mechanical test methods have been widely used for investigating the viscoelastic behavior of polymers. Storage modulus, *E*' determines the ability of the material to absorb or store energy; high storage modulus indicates more rigid material while loss modulus, *E*" determines the ability of a material to dissipate energy. The DMA results were obtained in terms of storage modulus, *E*' and loss modulus, *E*'' from -30 ^{o}C to 90 ^{o}C and presented in Figure 5.1 to Figure 5.4.

5.2.1 Storage modulus and loss modulus

Figure 5.1 shows the variation of storage modulus and loss modulus with temperature for pure RLDPE at different frequencies.

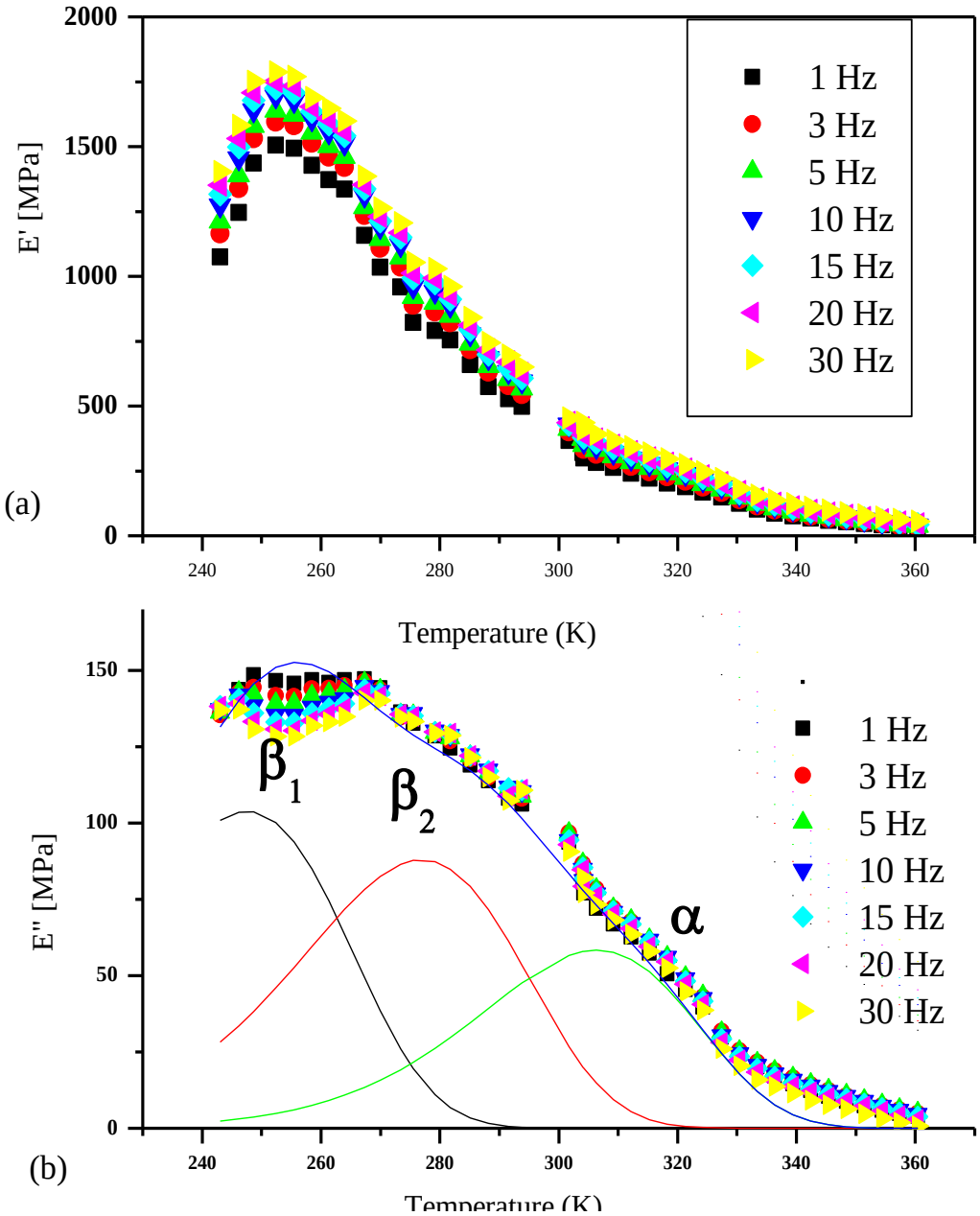

Figure 5.1 (a) Temperature dependence of the storage modulus of pure RLDPE (b)Temperature dependence of the loss modulus of pure RLDPE at the seven different frequencies studied. Solid lines are fit lines according to equation 3.7.

Figure 5.1 (a) shows that storage modulus increases with increase in frequency. At high frequency (shorter period) the sample behave like elastic solid while at low frequency (longer period) it's rubbery. E' decreases with temperature above 253 K indicating softening of the material when heated.

As the temperature is increased the polymer softens and large segmental motions in the amorphous regions become possible. The DMA results clearly show the validity of the time temperature superposition for the considered polymers. The effect of temperature increase on the viscoelastic properties is equivalent to the effect of time increase in a logarithmic scale, and the time is the inverse of the oscillation frequency. As a result, storage modulus decreases by increasing the temperature and increases with increasing the frequency.

Figure 5.1 (b) shows plots of loss modulus *E*'' against temperature for a pure sample at different frequencies. In the loss moduli obtained by DMA, the peaks corresponding to the β_1, β_2 and α transitions are clearly seen. The α- process is associated with large scale chain motion where as β_1 and β_2 suggest lamellae of two different thicknesses i.e β_1 and β_2 transitions are associated with branching relaxation or interlamellar shearing (Munaro *et al.,* 2008). From the graph, the loss modulus reduces with simultaneous increase in frequency. The decrease of loss modulus intensity as the frequency increases in Figure 5.1(b) can be attributed to the fact that at low frequencies, almost all the chains are able to follow the movement of the oscillations. This results into a resonance with a very high value of loss modulus. However, at higher frequencies it becomes very difficult for all the

chains to follow the movements of the oscillations. A few with shorter average chain length would be able to oscillate thus giving a lower value of loss modulus.

The polymer softens with simultaneous increase in temperature implying that more chains took part in the oscillation giving a higher value of loss modulus, but this is not the case. The crystallites impose chain constraints, which reduce the number of chains participating in the relaxation process, thus decreasing the loss modulus. Therefore, an increase in temperature in RLDPE makes the relaxation process becomes faster due to softening of the polymer and decreases the intensity due to chain constraints imposed by crystallization. However, this crystallization effect takes precedence. The convergence of the higher temperature tails of the loss moduli with increase in temperature is attributed to the changes in the crystallization process. This makes chain response at higher temperatures at all frequencies to be similar thus leading to convergence.

Figure 5.2 shows the temperature dependence of storage modulus *E*' and loss modulus *E''* for blends of different compositions at a frequency of 1 Hz.

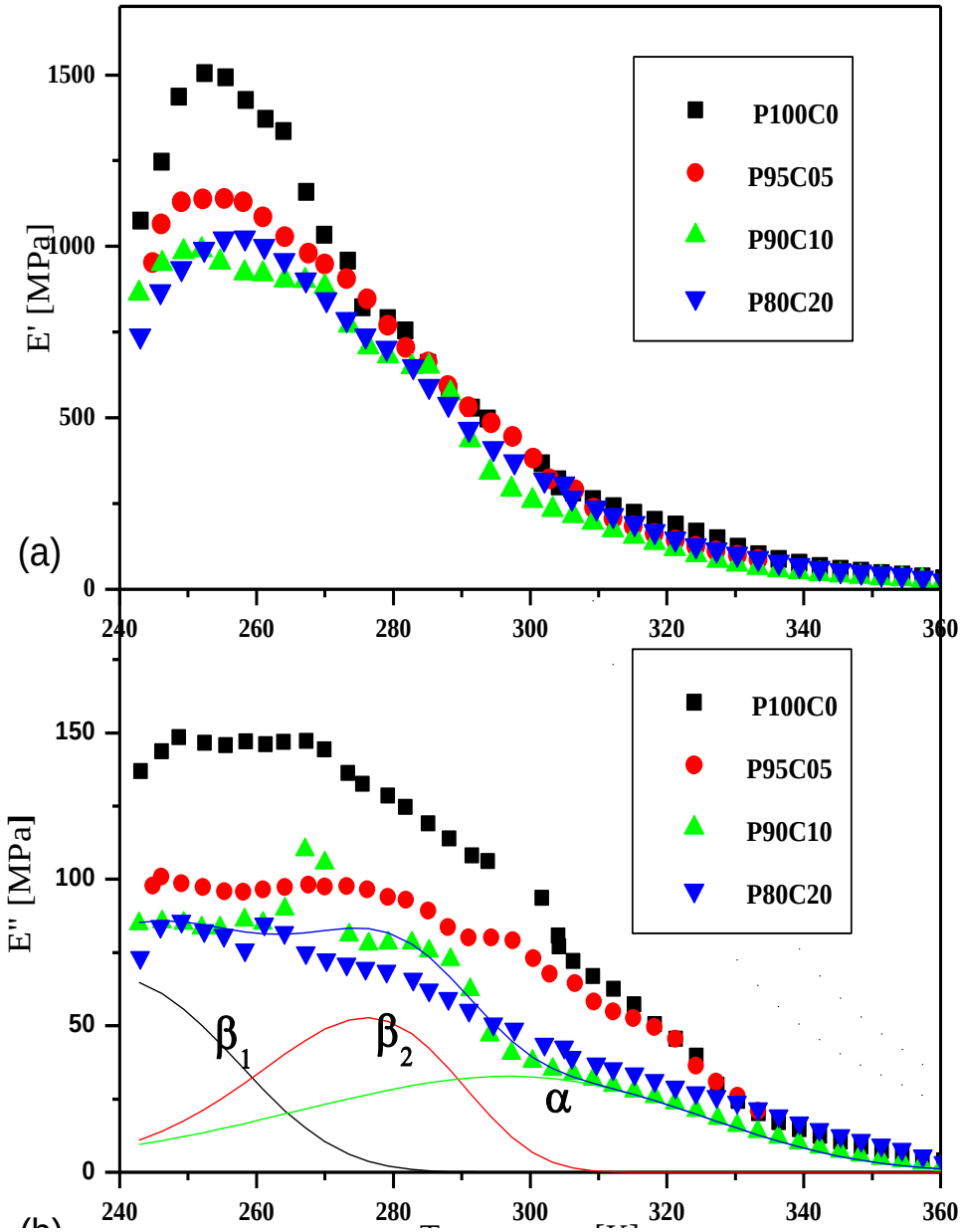

Figure 5.2 (a): Storage modulus as a function of temperature for RLDPE-CEL blends at 1 Hz. (b): loss modulus as a function of temperature for RLDPE-CEL blends at 1 Hz. Solid lines are fit lines according to equation 3.7.

It can be observed that the storage moduli of the blends were lower than those of the corresponding pure RLDPE. R/C blends also display three transitions as pure sample. E' decreased with CEL intake showing that the blend stores less energy on impact. T_α does not change with C intake meaning it does not change the free volume. Also T_β does not change with C intake due to lamellar stresses.

At lower temperatures, motion of CEL particles at the contact points is possible because of the high modulus of the matrix (Lee and Nielsen, 1977). The contribution of the interface to the modulus of the composites is much higher at higher temperatures than at lower temperatures (Hotta and Paul, 2004 ; Huang *et al.*, 2004). These results indicate that the incorporation of CEL has decreased the stiffness of the blends.

CEL therefore acts as a nucleating agent leading to a faster crystallization of RLDPE hence making the whole molecular environment rigid to motions. The crystallization speeds up due to nucleating effect of the CEL which is more pronounced and supersedes the temperature dependence crystallization. Therefore to relieve stresses, the induced chain stiffness results in large chain segments taking part in the relaxation process hence decrease in intensity.

5.3 CREEP ANALYSIS

The presence of CEL changes volume fraction that affect the creep behavior of blends. The other constants include CEL aspect ratio, CEL orientation (as a result of the processing), and mechanical properties of the CEL.

5.3.1 Effect of temperature on creep compliance and recovery

For all the samples examined the viscoelastic creep and recovery data were obtained under constant stress. The creep behavior of RLDPE-CEL blends as a function of time at different temperatures is shown in Figures 5.3.

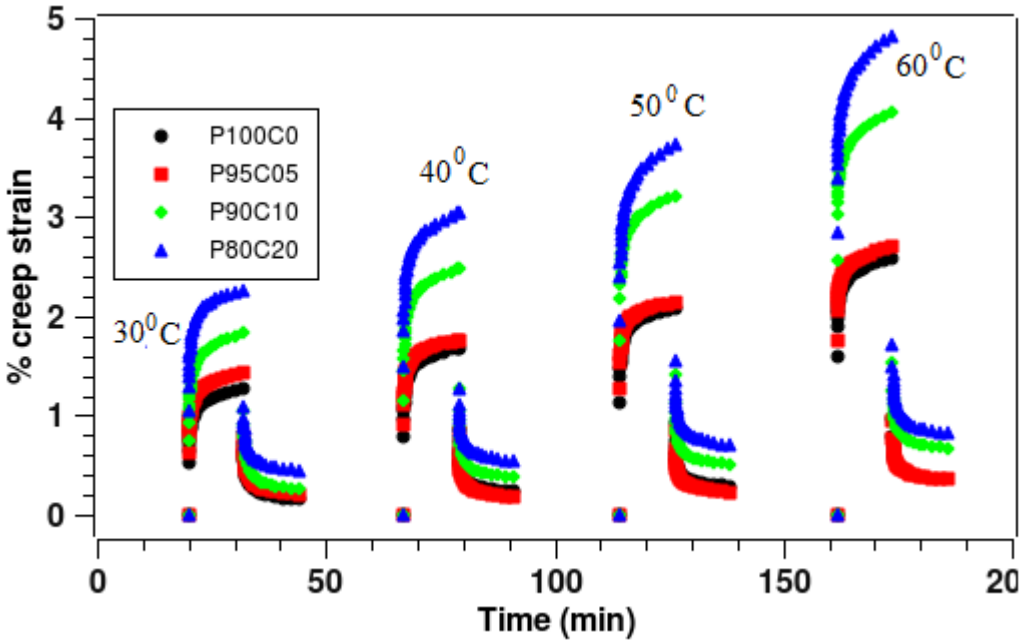

Figure 5.3: % creep strain of RLDPE- CEL blends as a function of time at different temperatures

It can be seen from the results that as temperature is increased the creep strain increased and the material recovered. This is due to increasing polymer chain mobility with increase in temperature and reduced entanglement. It can also be seen that increase in CEL decreases resistance to creep implying increased deformation. Recovery decreased with increase in temperature showing that disentangled chains can regain entanglement state. On the other hand, recovery increased with C intake because of the attraction due to the OH groups.

5.3.2 Time-temperature superposition

Figure 5.4 shows the isothermal curves of creep modulus. The value of creep modulus of all samples examined decrease with time. The isothermal curves provide the possibility of predicting the creep modulus and useful life of our blend materials in a wide range of time and temperature (Mehdi *et al.*, 2005). The curves show effects of time on the creep modulus of RLDPE-CEL blends. At short time intervals the materials examined exhibit a relatively high creep modulus.

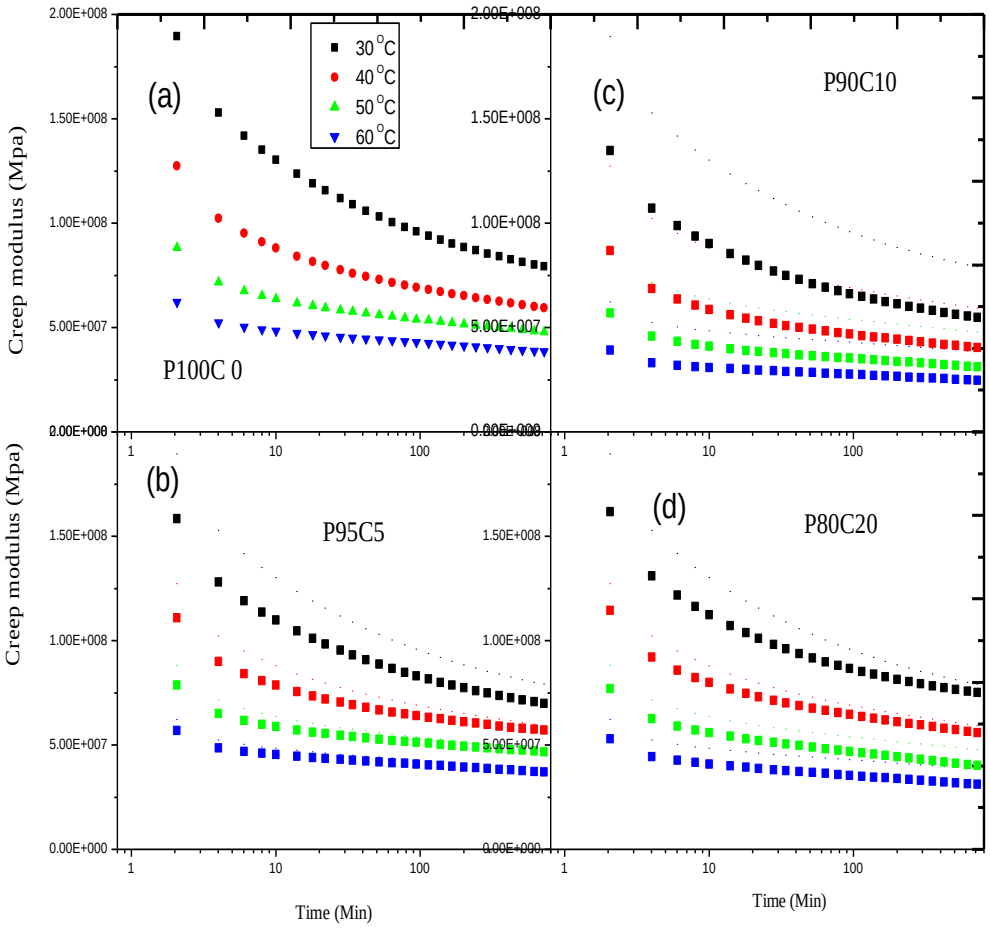

Fig 5.4: Creep modulus isothermal curves for all blends at 30, 40, 50 and 60 ^{o}C.

By selecting as the reference the curve for 30 ^{o}C, and then shifting all other isothermal curves of the creep modulus versus time obtained at 40 ^{o}C, 50 ^{o}C and 60 ^{o}C with respect to time, the curves of creep modulus versus time at reference temperature are generated as shown in Figure 5.7.

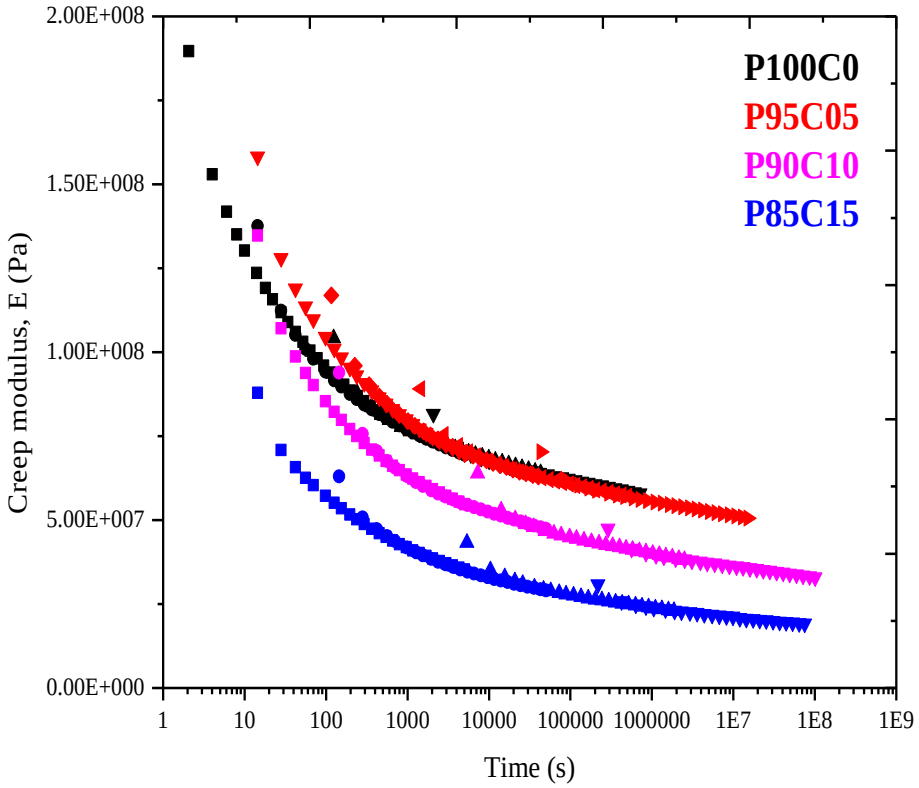

Figure 5.5: Creep modulus master curves for all blends at 30, 40, 50 and 60 ^{o}C.

The creep modulus, E, versus time curves are shifted to lower values with an increase of the CEL. At longer times viscous flow occurs and the materials exhibit a relatively low creep modulus. The results can be explained as follows: Under constant load, CEL undergoes molecular relaxation and rearrangement. The process involved in molecular rearrangement become more pronounced with time and are faster at higher temperatures. They are time and temperature dependent.

The experimental data for the shift factors, a_T were tested with WLF model equation 3.12 and shown in Figure 5.6.

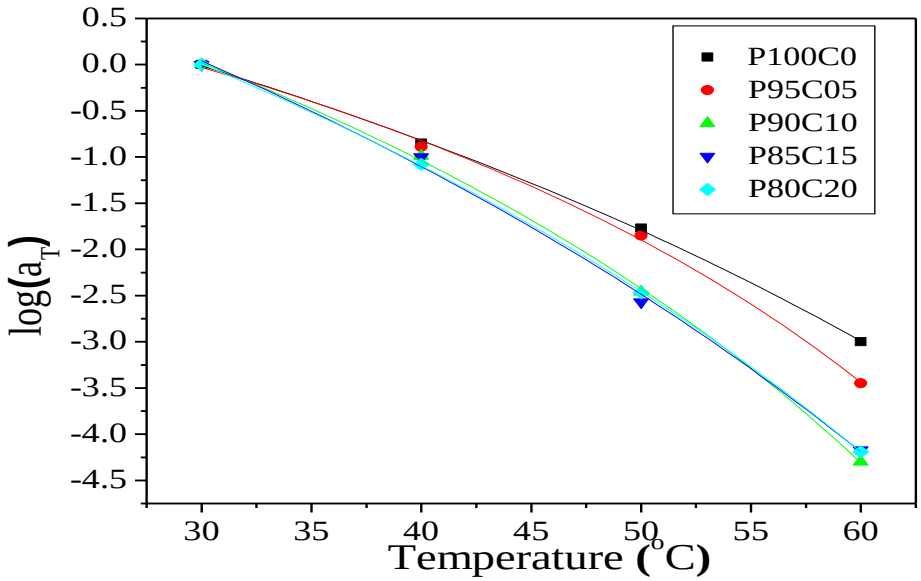

Figure 5.6: Activation plot for creep modulus. Solid lines are fits according to equation 3.12.

The results show good agreement with the WLF model. The shift factors decrease with CEL loading. The activation plot also shows that creep is dependent on free volume since the graph is not a straight line. Deformation of the blends depends on large chain segments. The fitted parameters are shown in the Table 5.1. C_1 and C_2 are constants while T_O is the reference temperature in ^oC.

Table 5.1: WLF activation parameters for various concentrations of CEL.

% CEL	C_1	C_2	T_O
0	-9	-117	29.8
5	-5	-76.7	29.6
10	-8	-85	30.2
15	-12	-115	30.4
20	-10	-104	30.1

5.4 Diffusion

The results for water uptake of RLDPE-CEL samples are shown in figure 5.9.

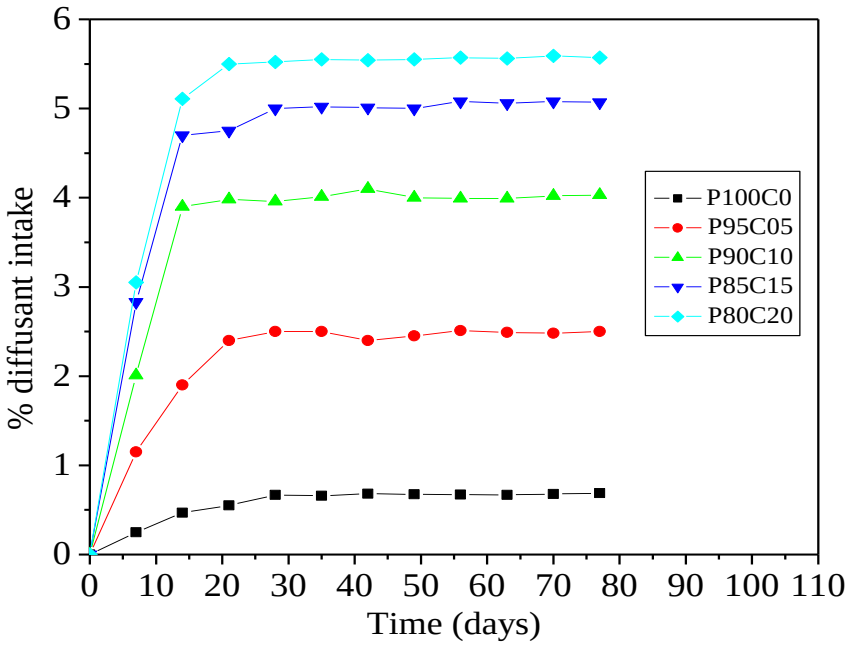

Figure 5.7: Variation of percentage weight of RLDPE-CEL blends with time.

RLDPE exhibited reasonably good water resistance compared to RLDPE-CEL blends. The percentage weight gained by the RLDPE-CEL samples over a period of 77 days when immersed in water is explained. In the first 7 days, the pure RLDPE absorbed only 0.27 % of water; however, the RLDPE-CEL of 95:5 blends absorbed 1.3 % of water in the first week. The water absorption slowly increased over a period of the 28 days, by which time the blends containing 0, 5, 10, 15 and 20 % CEL absorbed 0.5, 2.5, 4.0, 5.0 and 5.5 % of water, respectively. Water intake increased with time and CEL loading meaning the OH groups in CEL provided hydrophilic environment thus more water was absorbed.

Figure 5.10 shows the variation of M/M_{max} of pure RLDPE and RLDPE-CEL blends as

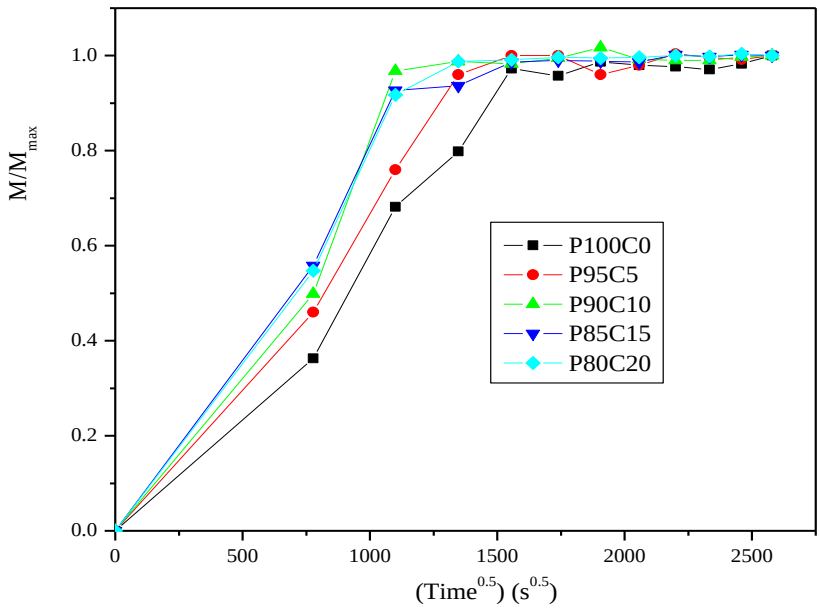

Figure 5.8: Effects of CEL on the moisture uptake of RLDPE blends during water absorption at room temperature.

a function of square root of time, $t^{0.5}$ at room temperature. The relationship between M/M_{max} and $t^{0.5}$ is an increasing gradient in each case, followed by saturation. A rapid moisture sorption was observed for all the specimens within the first few days of immersion. The absorption of water is related to its rate of diffusion into the blends. Figure 5.10 shows that the moisture intake increased with CEL loading.

5.4.1 Diffusion coefficient

CEL affects the water diffusion rate into the blends significantly because the water molecules get into the cellulose through cellulose- matrix interface. To understand this effect, diffusivity, *D* of water in the RLDPE-CEL blends specimens was determined by use of equation 3.54. M/M_{max} was plotted against $t^{\frac{1}{2}}$.

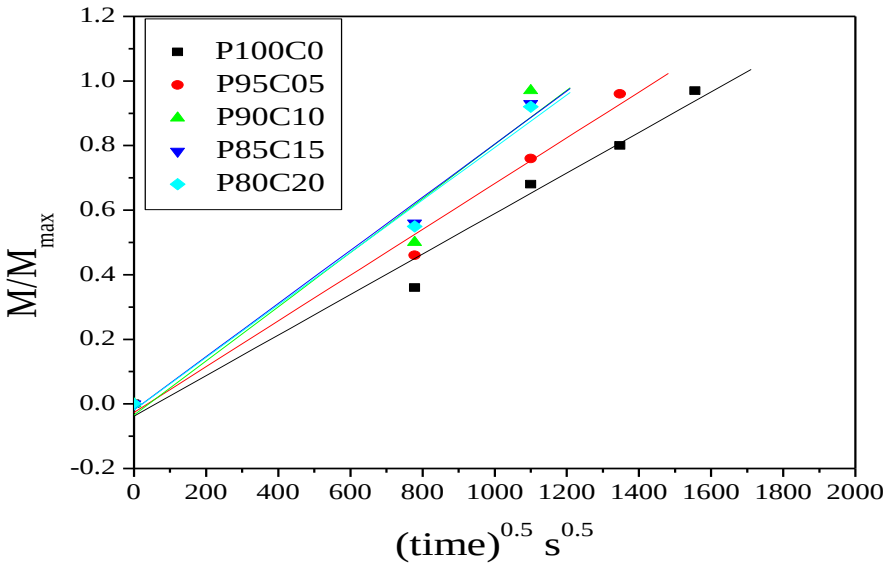

Figure 5.9: The effect of CEL concentration on the diffusion coefficient (*D*) of RLDPE blends at room temperature.

The diffusivity was determined from the initial slope of the plot in figure 5.11. The Table 5.2 below shows values of diffusivity, D of blends with different percentages of CEL concentration.

Table 5.2: Diffusivity values of RLDPE-CEL blends.

% CEL	D (cm^2/s)
0	$6.04x10^{-10}$
5	$7.26x10^{-10}$
10	$9.55x10^{-10}$
15	$1.06x10^{-9}$
20	$1.05x10^{-9}$

Diffusivity increases with CEL loading due to highly polar OH groups in the matrix enabling hydrogen bonding with water molecules hence increased water uptake. The water molecules could saturate the surface of the RLDPE-CEL composites easily and also penetrate into the blend through voids, resulting in higher water absorption in a short exposure time. Water absorption dropped slightly as immersion time was increased, owing to the fact that some CEL particle was leached away from the specimen (Ke *et al.,* 2003).

The value of diffusion coefficient of RLDPE is in agreement with the one reported by Me´tayer *et al* (1999). Diffusivity increases with increase in CEL concentration in the blend.

5.5 Thermal degradation

5.5.1 Thermal stability of blends

Thermal stability of RLDPE–CEL blends for different application is necessary in determining their temperature range of use and combustibility of compositions. Figure 5.12 presents the TGA experimental data for RLDPE–CEL blends.

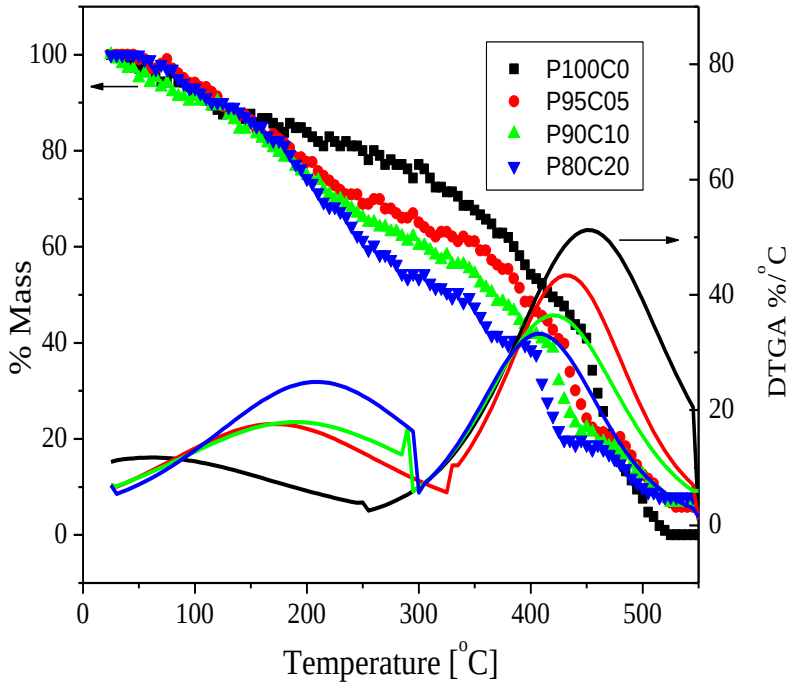

Figure 5.10: Thermogravimetric and derivative thermogravimetric curves of RLDPE blends.

RLDPE/CEL blends shows two- step degradation. The first stage is characterized by random scission /branching and breakage of glucosidic linkage in CEL while the second stage is due to decomposition of RLDPE. The peak decomposition temperature for the first stage increases with increasing CEL intake due to increase in glucosidic linkages. On

the other hand, peak decomposition temperature for the second stage decreases with increasing CEL intake due to decrease in RLDPE backbone which shows a decrease in thermal stability. Also the ash content increased with increase with CEL showing presence of less toxic byproducts of RLDPE. The mass loss of RLDPE started at 25 ºC and continued very slowly at temperature below 530 ºC. Above 530 ºC, the quantity of RLDPE residue was very low (equal 0.01%) due to further breakdown into gaseous products at higher temperature. In addition, as shown in Figures 5.12, the RLDPE- CEL blends exhibited initial mass loss from approximately 25 to 300 ºC, which was mainly due to the decomposition of CEL. After that, the second thermal degradation step of RLDPE-CEL was observed from 300 to 530 ºC. This finding seems to be in agreement with Behjat *et al* (2009).

The radical mechanism of RLDPE thermal degradation has been discussed as an example for random chains scission type reactions (Poutsma, 2003). The products of decomposition include a wide range of alkanes and alkenes and dienes. The kinetics of thermal degradation of LDPE which is expected to be the same as that of RLDPE is frequently described by a first-order model of mass conversion of the sample (Bockhorn *et al.,* 1999).

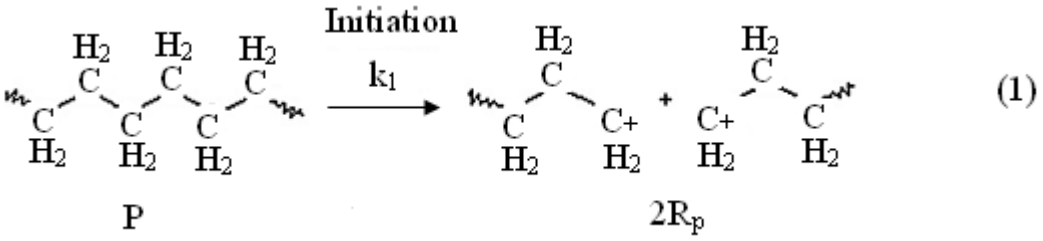

(1)

Propagation

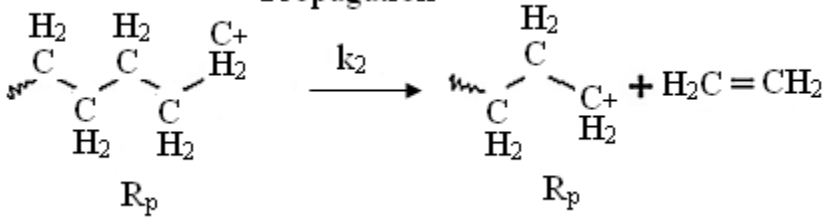

R_p R_p (2)

Hydrogen transfer (Intramolecular)

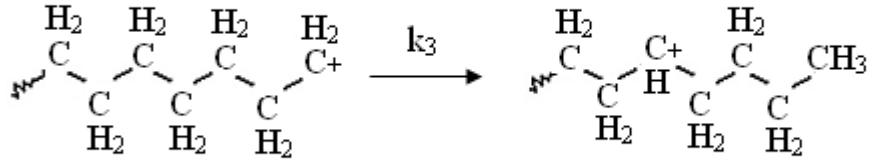

R_p R_s (3)

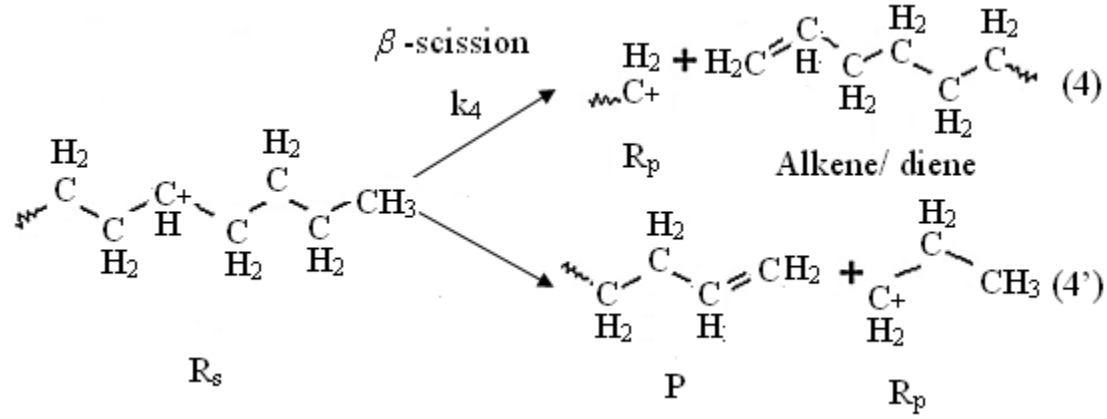

R_s R_p Alkene/ diene P R_p (4) (4')

Hydrogen transfer (Intermolecular)

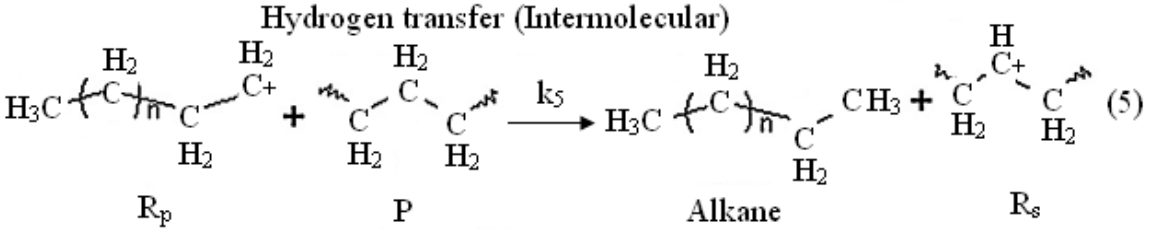

R_p P Alkane R_s (5)

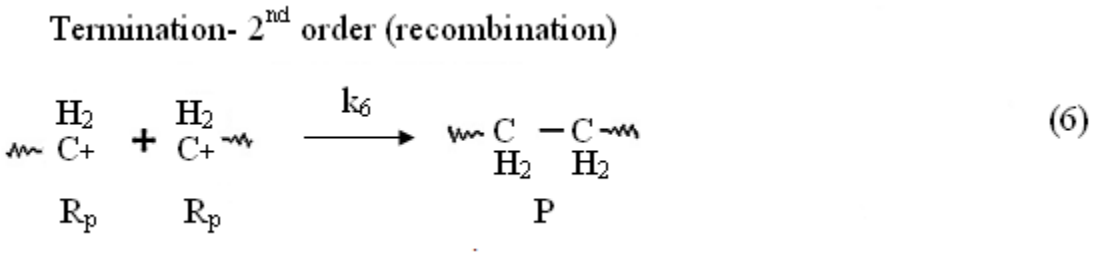

Scheme 5.1. Mechanism of RLDPE thermal degradation (Hornung *et al.*, 1998)

The reaction mechanism shown in scheme 5.1 considers only the main reactions in order to evaluate a simple kinetic model explaining the determined global kinetic data. The mechanism of RLDPE thermal degradation is a radical chain mechanism (Scheme 2), initiated by random scission of the polymer chain into primary radicals R_p (1). β-Scission of these radicals leads to ethylene (2). However at higher temperatures, the unzip reaction to ethylene is more evident (Bockhorn *et al.*, 1999). At lower temperatures, intermolecular hydrogen transfer followed by β-scission occurs (3). This reaction leads to the more stable secondary radicals R_s.

Subsequent β-scission of the secondary radicals contributes to the radical chain mechanism because the primary radical is produced in each step (propagation). Two β-scission reactions (4, 4') are possible. Reaction (4) leads to alkenes, whereas reaction (4') leads to a short primary radical and a polymer with a terminated double bond. Important for the change in the reaction order is the intermolecular hydrogen transfer in reaction (5), which leads to the alkanes. In this case only the intermolecular hydrogen transfer of the primary radicals is considered because they are less stable than the secondary radicals. At high

temperatures and at a high degree of conversion, alkane formation via reaction 5 is favored (Hornung *et al.,* 1998).

The thermal degradation of CEL involves at least four processes in addition to simple desorption of physically bound water (Beyler and Hirschler, 2002). The first is the cross linking of CEL chains, with the evolution of water (dehydration). The second concurrent reaction is the unzipping of the CEL chain (transglycosidation). Levoglucosan is formed from the monomer unit (Scheme 5.2).

The third reaction is the decomposition of the dehydrated product to yield char and volatile products. In addition, the levoglucosan can further decompose to yield volatile products and tars. Moreover, levoglucosan may also repolymerize. During CEL pyrolysis the inter chain ether formation. This process would generate a three-dimensional polymer more stable than CEL because the new ether bonds are more stable than the acetal-ether bonds.

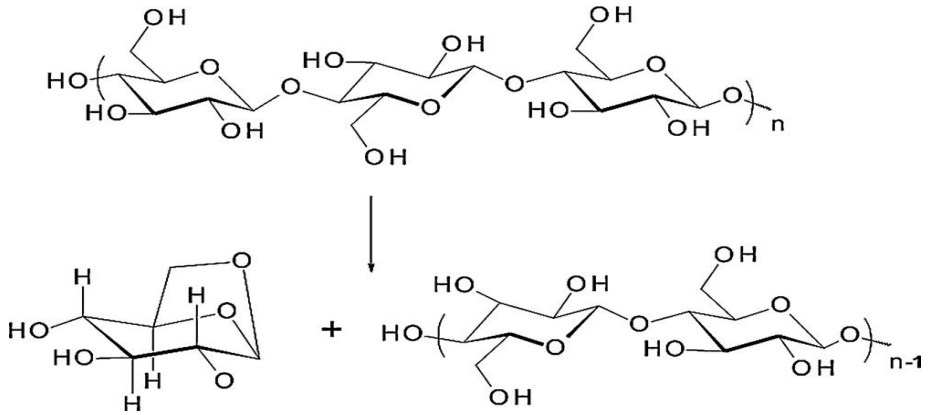

Scheme 5.2. Formation of levoglucosan via unzipping of the CEL chain

The increased thermal stability may allow further dehydration and possible dehydrogenation with less chain depolymerization and may be a step toward the char formation in cellulose pyrolysis. At higher temperatures (400 ºC) the cross-linked dehydrated cellulose and the repolymerized levoglucosan form polynuclear aromatic structures, and carbonaceous char.

5.5.2 Kinetic analysis of RLDPE-CEL blends for thermal degradation

Figure 5.13 shows the activation plots and kinetic parameters of thermal degradation of RLDPE- CEL blends. The values of activation energy of thermal degradation were obtained from the slopes of the two parts of the graphs.

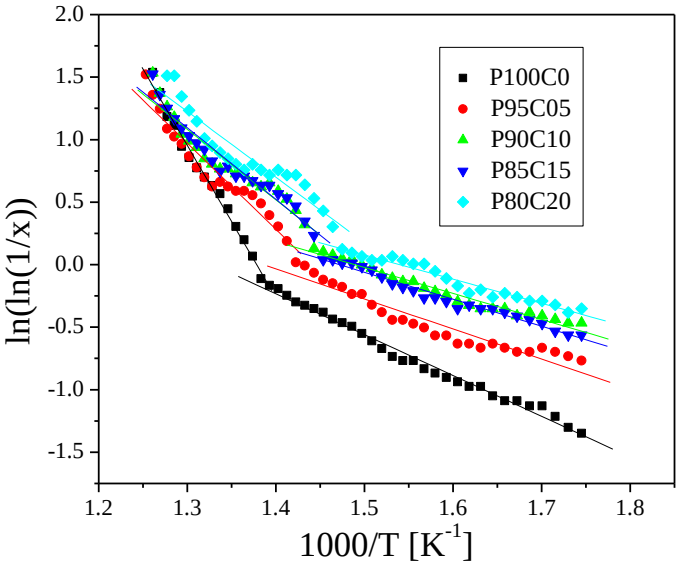

Figure 5.11: Activation plots and kinetic parameters of thermal degradation of RLDPE-CEL blends. Solid lines are fits according to equation 3.57.

The activation energy E_{a1} for pure RLDPE was 27.4 kJ/mol and it reduced with CEL loading. The activation energy Ea_2 for pure RLDPE was 101.4 kJ/mol and was found to reduce with CEL intake (Table 5.3).

Table 5.3: Kinetic parameters of thermal degradation of RLDPE-CEL blend

% CEL	E_{a1} (kJ/mol)	E_{a2} (kJ/mol)
0	27.4	101.4
5	19.9	57.3
10	17.5	46.5
15	18.3	47.4
20	15.8	44.0

Since $Ea_1 < Ea_2$; CEL decomposes at lower temperature than RLDPE. $E_{a\,2}$ decreases with CEL loading due to decrease in thermal stability.

5.6 Biodegradation

Figure 5.14 shows use of regression lines to obtain the lifespan of blends of the RLDPE-CEL blends buried in the alluvial soil. The rate of biodegradation increases with increase in cellulose content in RLDPE matrix. Full degradation times were obtained from the re-gression lines and given in table 5.4. Pure RLDPE was apparently almost completely ‘covered’ by RLDPE and thus was not accessible to microorganisms. On the contrary, in blends with a higher CEL content, the CEL was more exposed and consequently a greater portion of it was consumed by microbes.

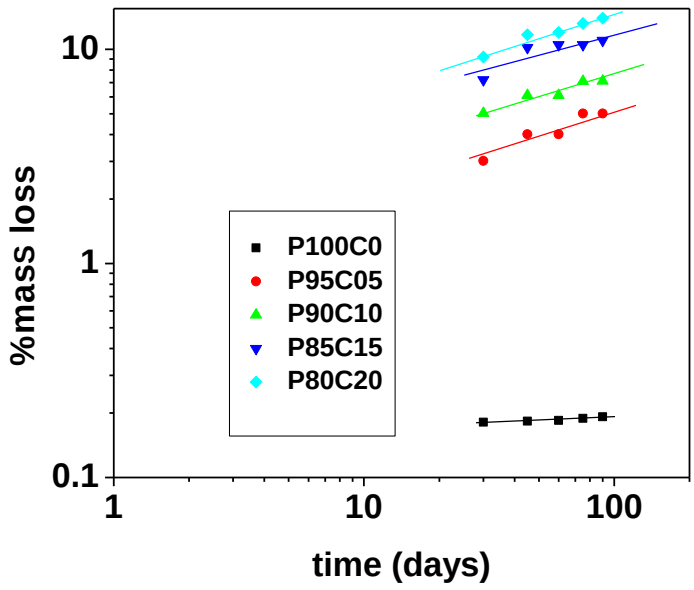

Figure 5.12: Percentage mass loss as a function of time for the RLDPE-CEL blends buried in the alluvial soil. Solid lines are fits according to $y = mx + c$.

This result shows close agreement with the analysis performed by Peanasky *et a1*(1991). According to these authors, microbial invasion took place from the top and bottom surfaces of the polymer films.

Table 5.4: Full degradation times of RLDPE-CEL blends

% CEL	Full deg time(yrs)
0	1459
5	8
10	7.6
15	5
20	3.5

Availability of highly polar hydroxyl groups in CELL increases hydrophilicity hence making the blend more compatible with microorganisms.

Biodegradation of RLDPE-CEL involves attachment of microorganism to the surface of the polymer, growth of microorganism utilizing the RLDPE-CEL as carbon source, primary degradation of RLDPE-CEL and ultimate degradation. Microorganisms can attach to the surface, if the polymer surface is hydrophilic. Since RLDPE have only the CH_2 groups, the surfaces are hydrophobic. Availability of highly polar hydroxyl groups in CEL increases RLDPE hydrophilicity hence making the blend more compatible with the organisms. Once the organisms get attached to the surface, they start growing by using the whole blend as the carbon source. In the primary degradation, the main chain cleaves, leading to the formation of low molecular weight segments (oligomers), dimmers or monomers. The degradation is due to the extracellular enzymes secreted by the organism. These low molecular weight compounds are further utilized by the microbes as carbon and energy sources. Small oligomers may also diffuse into the organism and get assimilated. The ultimate products of degradation are CO_2, H_2O and biomass under aerobic conditions. Anaerobic microorganisms can also degrade these polymers under anoxic conditions. The primary products then are CO_2, H_2O, CH_4 and biomass under methanogenic condition or H_2S, CO_2 and H_2O under sulfidogenic condition. The environmental conditions decide the group of microorganisms involved. Ultimate degradation of pure RLDPE takes 1459 years (Kawai *et al.,* 2002).

CHAPTER SIX

CONCLUSIONS AND RECOMMENDATIONS

6.1 Conclusions

Based on this study, there is an effective conclusion that CEL strongly affected the physical and mechanical properties of RLDPE-CEL blends. Results of this study suggest that CEL can be potentially attractive thermoplastic filler with RLDPE. The storage modulus of RLDPE was 1500 MPa at 1 Hz and 1750 MPa at 30 Hz while loss modulus was 150 MPa and 125 MPa respectively at a temperature of 250 K. The storage modulus of pure RLDPE and P80C20 were 1500 MPa and 1000 MPa respectively at 1 Hz. The loss modulus at 1 Hz was found to be 150 MPa and 75 Mpa for pure RLDPE and P80C20 respectively at 250 K. Three relaxation processes were detected using DMA. The intensity of the moduli decreased with CEL loading. No transition temperature, T_α and T_β shifts were observed. The effect of CEL loading level on creep property of RLDPE-CEL blends was investigated. The WLF model was able to characterize creep property of the bends for long-term prediction purposes and showed that deformation depends on free volume. CEL decreases resistance to creep.

The water absorption behavior of RLDPE-CEL blends has been investigated with special reference to CEL loading. The kinetics of water absorption of the RLDPE-CEL blends conforms to Fick's law of diffusion. The *D* values range from 6.04×10^{-10} cm/s^2 for pure RLDPE to 1.05×10^{-9} cm/s^2 for P80C20. This shows that the uptake of water increases with CEL loading. RLDPE-CEL blends are therefore promising permeable membranes.

Thermal properties of RLDPE-CEL blends have been investigated. The blends showed two stage degradation due to RLDPE (decomposition of its low and high molecular weight fragments) and CEL (cross-linking and unzipping of the CEL chain). The activation energy for thermal degradation was found to range from 27.4 kJ/mol for pure RLDPE to 15.8 kJ/mol for P80C20 during the first step of degradation and 101.4 kJ/mol to 44.0 kJ/mol for P80C20. The full biodegradation times of pure RLDPE and P80C20 were found to be 1459 years and 3.6 years respectively. Addition of CEL has increased the biodegradability characteristics of RLDPE wherein microbes assimilate the CEL particles and leave the RLDPE matrix alone with the weaken bonding of polymer chains. The breakdown of the RLDPE chains down into small particles with a large surface area follows. RLDPE-CEL blends are therefore promising non environmental plastic pollutants.

6.2 Recommendations

More extensive experimental work should be done to characterize the material over a wider range of temperature. A temperature range of -90 ^{o}C to 100 ^{o}C would help in determining the widest range of operating temperature. It would also be necessary to carry out similar studies using higher percentages of CEL concentration in the blend. Supplementing the measurements using techniques like the scanning electron microscopy, (SEM), attenuated total reflection (ATR) infrared, or X-ray diffractometry to study the structure of the samples would be appropriate. This may give a more accurate explanation of the molecular dynamics of the sample blends. These blends should be adopted by policy makers in a bid to reduce environmental pollution.

REFERENCES

Alamri, H. Low, I. Alothman, Z. (2012). ‘‘Mechanical, thermal and microstructural characteristics of cellulose fibre reinforced epoxy/organoclay nanocomposites’’*Journal of polymer science,* **Volume 21:** 1-10.

Alcock, B. Cabrera, N. Barkoula, N. Wang, Z. Peijs, T. (2008). ‘‘The effect of temperature and strain rate on the impact performance of recyclable all-polypropylene composites’’ *Journal of polymer science,***Volume 39**: 537–547.

Alhuthali, A. Low, M. Dong, C. (2012). ‘‘Characterisation of the water absorption, mechanical and thermal properties of recycled cellulose fibre reinforced vinyl-ester eco-nanocomposites’’ *Journal of polymer composites,* **Part B**: 1-10.

Anamaria, S. Raluca, N. Marian, T. Georgeta, C. Cornelia, V.(2012). ‘‘Low density polyethylene composites containing cellulose pulp fibers’’ *Journal of polymer science,* **Volume 43**: 1873–1880.

Averous, L. and Boquillon, N. (2004).‘‘Carbohydrate Polymers’’. *Journal of Polymer Degradation and Stability,* **Volume 56**: 111-122.

Aroni, S., Mrinal, B., Kim, A., Stelson, P. and Vaughan, R. (2001). *Creep in injection molded starch/synthetic polymer blends.* University of Minnesota, U.S.A.

Arutchelvi, J. Sudhakar, M, Ambika, A. (2008). “Biodegradation of Polyethylene and Polypropylene” *India journal of Biotechnology*, **Volume 7**: 9-22.

Arvanitojannis, J. (1999). ‘‘Totally and partially biodegradable polymer blends based on natural and synthetic macromolecules’’. *Journal of Macromolecular Science,* **Volume 39**: 205-271.

Behjat, T. Russly, A. Luqman, C.Nor, A. and Yus, A. (2009). “Thermal Properties of Low Density Polyethylene - Filled Kenaf Cellulose Composites” *European Journal of Scientific Research*, **Volume 32**: 223-230.

Bernasconi, A. Rossin, D. Armanni, C. (2007). ‘‘Analysis of the effect of mechanical recycling upon tensile strength of a short glass fibre reinforced polyamide 6,6’’. *Journal of Engineering Fracture Mechanics,* **Volume 74**: 627–641.

Beyler, C.L. Hirschler, M.M. (2002). “Thermal decomposition of polymers”. SFPE Handbook of Fire Protection Engineering, 3rd ed., National Fire Protection Association, Quincy, MA, pp. 1-110.

Beyer, L. and Marcelo, H. (2009). ‘‘Thermal decomposition of polymers’’. *Journal of fire protection engineering,* **Volume 31**: 110–120.

Bikiaris, D. and Panayiotou, C. (1998). ‘‘LDPE/starch blends compatibilized with PE-g-MA copolymers’’. *Journal of Applied Polymers Science,* **Volume 70**: 1503-1521.

Billmer, W. and Fred, J. (1984). ‘‘Textbook of polymer science’’. 3rd Edition. pp 366-367.

Broido, A. (1969). ‘‘A simple, sensitive graphical method of treating thermogravimetric analysis data. *Journal of Polymer Science,* **Volume 2**: 1761.

Bodor, G. (1991). ‘‘Structural investigation of polymers’’. 4th Ed, pp 194-199.

Bockhorn, H. Hornung, A. and Hornung, U. (1999) ‘‘Mechanisms and kinetics of thermal decomposition of plastics from isothermal and dynamic measurements’’. *Journal of Analytic Applied Pyrolysis,* **Volume 50**: 77-101.

Chandra, R. and Renu, R. (1997) ‘‘Biodegradation of maleated linear low-density polyethylene and starch blends’’ *Journal of Polymer Degradation and Stability,* **Volume 56**:185-202.

Cheng, X., Shi, H., Adams, C. and Ma, Y. (2010). ‘‘Assessment of metal contaminations leaching out from recycling plastic bottles upon treatments” *Journal of environmental science and pollution research international,* **Volume 17**: 1323-1330.

Cowle, J. M. (1991). ‘‘Polymer chemistry and physics of modern materials’’. 2nd Ed. pp 226-227.

Coutinho, F., Costa, T., Suarez, J. and Melo, D. (2000). ‘‘Sawdust reinforced polypropylene composites: a study of fracture behaviour’’. *Journal of Polymer Testing*, **Volume 19**: 625-633.

Crank, J.J. (1975). ‘‘The mathematician of diffusion’’. United Kingdom: Oxford University Press, 100-165.

Crawford, R.L. (1981). ‘‘Lignin biodegradation and transformation’’. New York: Cambridge University Press, pp 30- 85.

Dave, H. Rao, PVC and Desai, J. (1997). ‘‘Biodegradation of starch polyethylene films in soil and by microbial cultures’’. *World Journal of Microbiological Biotechnology*. **Volume 13**: 655-658.

David, H. Elisabeth, H. Peter, J. Ian, M. and Richard, A. (1996). ‘‘The cure and diffusion of water in halogen containing Epoxy/amine thermosets’’. United Kingdom: Defense Research agency, 69-80.

Devi, L., Bhagawan, S., and Thomas, S. (1997). *Journal of Applied Polymer Science*, **Volume 64** :1739.

Doolittle, A. K. and Doolittle, D. B.(1957). *Journal of applied physics*. **Volume 28**:901

Eleni, P, Ioannis, A, Costas, G, Biliaderis, C, Hiromasa, O. and Norioki, K. (1998). ‘‘Carbohydrate Polymers’’ *Journal of Thermoplastic carbohydrates.* **Volume 36**: 89-104.

Findley, W.N. Lai, J.S. and Onaran, K. (2007). ‘‘Creep and relaxation of nonlinear viscoelastic materials with an introduction of linear viscoelasticity’’. Dover publications, Inc., New York.

Friedman, H.L. (1965). “Kinetics and gaseous products of thermal decomposition of polymers”. *Journal of Polymer Science.* **Volume 6**: 183-195.

Fugita, H. (1968). ‘‘Diffusion in polymers’’. New York: Academic press, pp 20-84.

George, J. Bhagawanb, S. S. and Thomas, S. (1998) “Effects of environment on the properties of low-density polyethylene composites reinforced with pineapple-leaf fibre” *Journal of Composites Science and Technology*. **Volume 58**: 1471-1485.

Girija, B.G., Sailaja, R.R.N. and Giridhar, M. (2005). ‘‘Thermal degradation and mechanical properties of PET blends’’ *Journal of Polymer Degradation and Stability*. **Volume 90**: 147-153.

Groeninckx, G., Chandra, S., Berghmans, H., and Smets, G. (1979). ‘‘Morphology, Viscoelastic properties, and Stress-Strain behavior of blends of polycarbonate of Bisphenol – A and Atactic polystyrene’’ *Journal of Polycarbonate–cellulosic fibers composites.* **Volume 58**: 1221-1267.

González, C. Fonseca, C, Ochoa, A. Garriga, A. and Rodríguez, E. (2011). ‘‘Rheological behavior of original and recycled cellulose–polyolefin composite materials’’. *Journal of polymer science.* **Volume 42**: 1075–1083.

Göran, G. Allan, H. and Kristiina, O. (2010). ‘‘Silane-crosslinking of recycled low-density polyethylene/wood composites Composites’’. *Journal of polymer science.* **Volume 41**:678–683

Hannequart J-P, (2004). Good practice guide on waste plastics recycling: A guide by and for local and regional authorities. Association of cities and regions for recycling (ACRR), Belgium.

Hakkarainen, M. and Albertsson, A. (2004). ‘‘Environmental degradation of polyethylene’’. *Advanced Polymer Science.* **Volume 169**: 177-199.

Harikumar, K., Joseph, K. and Thomas, S. (1999). ‘‘Jute sack cloth reinforced polypropylene composites: mechanical & sorption studies’’. *Journal of Reinforced Plastics and Composites*. **Volume 18**: 346-372.

Herrera, F. Pedro, J. and Valadez-Gonzalez, A. (2005)"Natural fibers, biopolymers, and biocomposites". *Journal of Polymer Degradation and Stability*. **Volume 6**: 177-230.

Hirata, T. Ringyo, S. and Kenkyu, H. (1974). ‘‘Effect of inorganic salts on pyrolysis of wood and cellulose, measured with thermogravimetric and differential thermal analysis techniques’’. *Journal of polymer degradation and stability*. **Volume 263**: 17-33.

Hornung, U. Hornung, A. and Bockhorn, H. (1998). ‘‘Investigation of thermal degradation of solids in an isothermal, gradient free reactor’’ *Journal of Chemical Engineering and Technology*. **Volume 21**: 332-337.

Hotta, S. and Paul, D.R. (2004). *Polymer*. **Volume 45**: 7639–7654.

Huang, Y. Q. Jiang, S. Libo, W. and Hua, Y.Q. (2004). *Polymer Testing.* **Volume 23**: 9-15.

Huang, S. Klingsberg, A. Muldoon, J. and Salvadore, A. (1985). Biodegradable polymers, in: (Eds.), Encyclopedia of Polymer Science and Engineering, Wiley, New York, 220-243, Part 2.

Huda, M. S. Mohanty, A. K. Drzal, L. T. (2005) “Green Composites from Recycled Cellulose and Poly(lactic acid): Physico-mechanical and Morphological Properties Evaluation’’ *Journal of Material Science.* **Volume 40**: 4221 – 4229.

Ioannis, A. Costas, G. Biliaderis, H. Ogawa, K. and Norioki, K. (1998). *Journal of Chemistry and Biochemistry*, **Volume 68**: 565-690.

Jiulin, X. and Wang, Z. (1999). ‘‘Holographic Grating Relaxation Studies of Probe Diffusion in a Polymer Blend’’. *Journal of polymer science.* **Volume 68**: 561-698.

Joseph, K. Thomas, S. and Pavithran, C. (1995). “Effect of ageing on the physical and mechanical properties of sisal-fiber reinforced polyethylene composites”. *Journal of Composite Science and Technology*. **Volume 53**: 99-110.

Kahovec, J. Fox, R. and Hatada, K. (2002). "Nomenclature of regular single-strand organic polymers" *Journal of Pure and Applied Chemistry*. **Volume 74**: 1921-1940.

Kamdem, D. Haihong, J. Weining, C. Jason, F. and Matuana, L. (2012). Properties of wood plastic composites made of recycled HDPE and wood flour from CCA-treated wood removed from service. *Journal of polymer science.* **Volume 43**: 1873–1880.

Kawai, F. Watanabe, M. Shibata, M. Yokoyuma, S. and Sudate, Y. (2002). “Experimental analysis and numerical simulations for biodegradability of PE” *Journal of polymer degradation and stability*. **Volume 76**: 129-135.

Ke, T. Sun, X. and Seib, P. (2003). ‘‘Blending of poly(lactic acid) and starches containing varying amylose content’’. *Journal of Applied Polymer Science*. **Volume 89**: 3639-3646.

Khalid, M. Ratnam, C. Luqman, A. Salmiaton, A. Choong, T. and Jalaludin, H. (2009). ‘‘Thermal and Dynamic Mechanical Behavior of Cellulose and Oil Palm Empy Fruit Bunch- Filled Polyproplyne Biocomposites’’ *Journal of Polymer- Plastics Technology and Engineering.* **Volume 48**: 1244-1251.

Kraiem, D. Pimbert, S. Ayadi, A. Bradai, C. (2012). ‘‘Effect of low content reed (Phragmite australis) fibers on the mechanical properties of recycled HDPE composites’’. **Volume 30**: 1-7.

Krishnan, J. and Rex, H. (2009) ‘‘Harakeke (phormium tenax) fibre–waste plastics blend composites processed by screwless extrusion’’ *Journal of Composites.* **Volume 40**: 645–649.

Kuroki, T. Sawaguchi, T. Niikuni, S. and Ikemura, T. (1982). ‘‘Mechanism for long-chain branching in the thermal degradation of linear high-density polyethylene, Macromolecules’’. *Journal of polymer science.* **Volume 15**: 1460-1462.

Lee, B. and Nielsen, L. (1977). *Journal of Polymer Science.* Phys Ed; **Volume 15**: 683–692.

Lee, S. and Wang, S. (2006). ‘‘Biodegradable polymers/bamboo fiber biocomposite with bio-based coupling agent’’. *Journal of Applied Science and Manufacturing*. **Volume 37**: 80-91.

Levchik, S. and Weil, E. (2006). ‘‘Polycarbonates and blends” *Journal of Flame retardants in commercial use or in advanced development in polycarbonates and polycarbonate blend.* **Volume** 24: 137-151.

Li, F. Larock, R. and Otaigbo, J. (1999). ‘‘Creep and recovery behavior” *Journal of Fish oil thermosetting.* **Volume 42**: 453-675.

Luo, X. Benson, S. Kit, K. and Dever, M. (2002). ‘‘Fibre reinforced polypropylene composite’’. *Journal of Applied Polymer Science*, **Volume 85**: 1961-1969.

Madsen, B. and Lilholt, H. (2003). ‘‘Composites Science and Technology” Journal of Physical and mechanical properties of unidirectional plant fibre composites- an evaluation of the influence of porosity, 63: 1265-1272.

Mamleev, V. Bourbigot, S. and Yvon, J. (2007). “Kinetic analysis of the thermal decomposition of cellulose” *Journal of Analytical Applied Pyrolysis*, **Volume 80**: 151-165.

Mamleev, V. Bourbigot, S. Le Bras and M. Yvon, J. (2009). ‘‘The facts and hypotheses

relating to the phenomenological model of cellulose pyrolysis'' *Journal of Analytical Applied Pyrolysis,* **Volume 84**: 1-17.

Marco, V. Fabrizio, S. Francesco, M. Jacopo, T. and Giovanni, P. (2012). ''Hybrid recycled glass fiber/wood flour thermoplastic composites: Manufacturing and mechanical characterization'' *Journal of polymer science,* **Volume 42**: 649–657.

McCrum, P. Buckley, N. and Bucknall, C. (2003). ''Mechanical Analysis of Polymers" *Journal of Principles of Polymer Engineering*, **Volume 19**: 856-526.

Mehdi, T., Robert, H. and John, C. (2005). "Hermanson Time–Temperature Superposition Principle Applied to a Kenaf-Fiber/High-Density Polyethylene Composite" *Journal of Applied Polymer Science*, **Volume 97**: 1995–2004.

Me´tayer, M. Labbe´, M. Marais, S. Langevin, D. Chappey, C. Dreux, F. Brainville, M. and Belliard, P. (1999). ''Test Method Diffusion of water through various polymer films: a new high performance method of characterization'' *Journal of Applied Polymer Science*, **Volume 11**: 533-549

Meyers, T. and Chawla, M. (1999). ''Mechanical behavior of polymers" *Journal of Mechanical behavior of Materials*, **Volume 13**: 570–580.

Mishra, A.K. and Luyt, A.S. (2008). ''Polymer Degradation and Stability'' *Journal of Applied Polymer Science*, **Volume 93**: 145-150.

Mohanty, A. Misra, M. Drzal, L. Selke, S. Harte, B. and Hinrichsen, G. (2005) "Natural fibers, biopolymers, and biocomposites." *Journal of Polymer Degradation and Stability,* **Volume 1**: 1-36.

Nishino, T., Takano, K. and Nakamae, K. (1995). ''Elastic Modulus of the Crystalline Regions of Cellulose Polymorphs''. *Journal of Polymer Science*: Part B: Polymer Physics, **Volume 33**: 1647-1651.

Opfermann, J. (2000). "Kinetic analysis using multivariate non-linear regression". *Journal of Thermal Analysis,* **Volume 60**: 641–658.

Peanasky, J. Long, J. and Wool, R. (1991). *Journal of Polymer Science,* **Volume 29**: 565.

Peng, H., Kawagoe, W. and Hogan, D. (2002). ''Sitosterol-beta-glucoside as premer for cellulose synthesis in plants'', pp 147-150.

Pielichowski, K. and Njuguna, J. (2005). ''Natural polymers''. *Journal of Thermal Degradation of Polymeric Materials,* **Volume 86**: 133–138.

Prut, E. and Zelenetskii, A. (2001). ''Chemical modification and blending of polymers

in an extruder reactor''. *Journal of polymer degradation and stability,* **Volume 70**: 65–79.

Poutsma, M. (2003). ''Reexamination of the pyrolysis of polyethylene: data needs, free-radical mechanistic considerations, and thermochemical kinetic simulation of initial product-forming pathways, Macromolecules''. *Journal of polymer science,* **Volume 36**: 8931–8957.

Ramazan, K., Basel, A. (2007). ''International Journal of Polymeric Materials, Moisture Absorption Behavior of Palm/Polypropylene Composites in Distilled Water and Sea Water''. *Journal of polymer science,* **Volume 56**:43–53,

Ratajska, M. and Boryniec, S. (1999). ''Biodegradation of some natural polymers in blends with polyolefins''. *Polymer Advanced Technology,* **Volume 10**: 625-633.

Rui, D., Yun, C., Pu, C., Lin, Z. and Bing, L. (2006). ''Properties and biodegradability of water-resistant soy protein/poly (ε-caprolactone)/toluene-2,4-diisocyanate composites'' *Journal on Degradation and Stability,* **Volume 91**: 2189-2197.

Russell, K., Edward, J. K. and Dwain, M. W. (2001). ''Fast macromolecules control mutual diffusion in polymer blends''. New York, USA, 867-965.

Sax, L. (2010). "Polyethylene Terephthalate May Yield Endocrine Disruptors" *Journal of Environmental Health Perspectives,* **Volume 118**: 567-765.

Scoponi, M. Cimmino, S. Kaci, M. (2000). ''Polymer'' p 7967.

Shotyk, R., William, K., Michael, C. and Bin, F. (2006). "Contamination of Canadian and European bottled waters with antimony from PET containers" *Journal of Environmental Monitoring*, **Volume 8**: 288-300.

Singleton, A. Baillie, C. Beaumont, P. and Peijs, T. (2003). ''On the mechanical properties, deformation and fracture of a natural fibre/recycled polymer composite''. *Journal of polymer science,* **Volume 34**: 519–526.

Sinha, R. S. and Bousmina, M. (2005). ''Progress in Materials Science.'' p 962–1079

Smith, W.F. (2004). ''Mechanical properties of materials''. New York: Cambridge University Press, 14-54.

Speight, J. G. and Norbert, A. (2005). ''Lange's handbook of chemistry'', 16th ed. McGraw-Hill. 2.807–2.758. ISBN 0071432205.

Sperling, L.H. (1992). ''Introduction to physical polymer science'' 2nd ed. 320-323

Suda, K. Prodepan, T. and Manit, S. (2001) ‘‘Chemical modification of cassava starch for degradable polyethylene sheets’’ *Journal of Polymer Degradation and Stability*, **Volume 73**: 363–375

Tsuchii, A. Suzuki, T. and Fukuoka, S. (1980). ‘‘Microbial degradation of polyethylene oligomers’’. *Rep.Ferment. Res. Inst.* **Volume 55**: 35-40.

Vauderschueren, J. and Gasiot, J.(1979). ‘‘Thermally stimulated relaxation in solids’’ sponger-verlag, Berlin. **Vol. 37**, chapter 4.

Vogel, A.(1921). Physics. 22: p645.

Ward, I. M. and Hadley, D. W. (1993). *‘‘*An introduction to the mechanical properties of solid polymers solids’’. Chapter 6, pp 96-100.

Wool, R. P. Peanasky, J. S. Long, J. M. and Goheen. S. M. (1989). In Proc. First Int. Scientific Consensus Workshop on Degradable Materials, Toronto. Canada, **Volume 4**: 515.

Wright, J. R. and Mathias, L. J. (1993) “Physical characterization of wood and wood polymer composites” *Journal of Applied Polymer Science*. **Volume 48**: 2225-2239.

Yanjun, X. Sun-Young, L. and Qinglin, W. (2011). ‘‘Creep Analysis of Bamboo High-Density Polyethylene Composites: Effect of Interfacial Treatment and Fiber Loading Level. Journal of polymer composites’’ *Journal of polymer science* .**Volume 12**: 130-712

Yang, H. Wolcott, M. and Kim, H. (2005). ‘‘Thermal properties of lignocellulosic filler-thermoplastic polymer bio-composites. *Journal of Thermal Anaysis Calorimetry*. **Volume 82**: 157-160.

Yew, G. Mohd, Y. and Mohd, I. (2005) ‘‘Water absorption and enzymatic degradation of poly(lactic acid)/rice starch composites*’’ Journal of Polymer Degradation and Stability*. **Volume 90**: 488-500

Zhao, G. Liu, Y. Fang, C. Zhang, M. Zhou, C. and Chen, Z. (2006) ‘‘Water resistance, mechanical properties and biodegradability of methylated-cornstarch/poly(vinyl alcohol) blend film’’ *Journal of Polymer Degradation and Stability*. **Volume 91**: 703-711

Zheng, Y. and Yanful, E.K. (2005) “A review of Plastic waste degradation” *Journal of polymer science*. **Volume 25**: 234-250.

APPENDICES

APPENDIX I: Photograph showing Acacia tree trunk and cell sap.

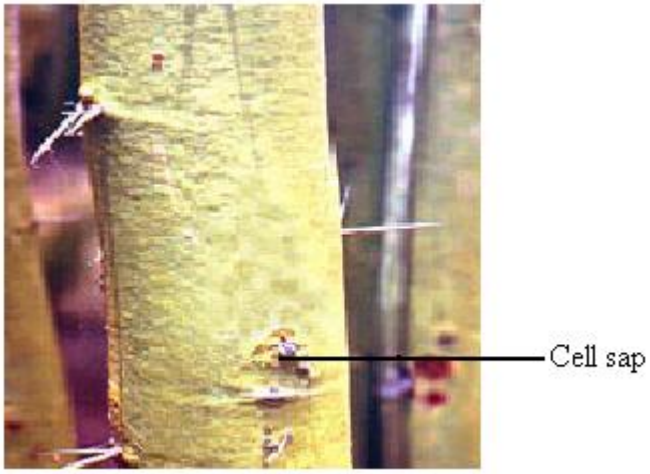

APPENDIX II: Photograph of complete DMA system.

APPENDIX III: Photograph of internal components of DMA 2980 TA machine

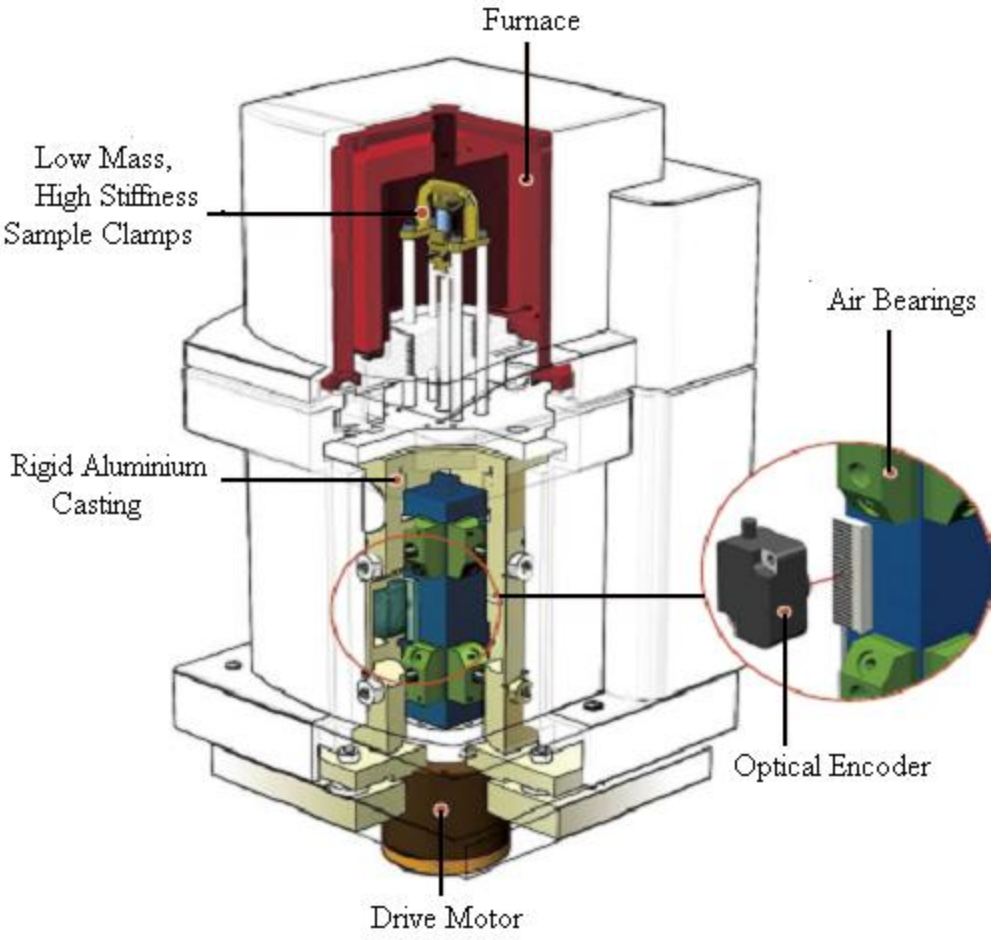

APPENDIX IV: Photograph of Single Cantilever Clamp selection.

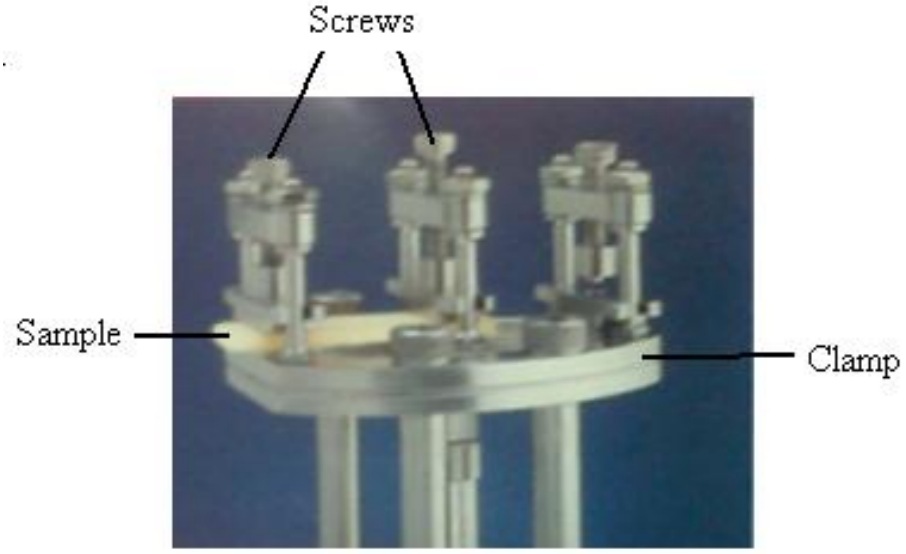

APPENDIX V: Photograph of a complete TGA system.